AD_____

Award Number: DAMD17-03-1-0285

TITLE: The Antemortem Detection and Conformational Switches of Prion Proteins

PRINCIPAL INVESTIGATOR: David Schubert, Ph.D.

CONTRACTING ORGANIZATION: Salk Institute for Biological Studies
La Jolla, CA 92037-1099

REPORT DATE: July 2006

TYPE OF REPORT: Final

PREPARED FOR: U.S. Army Medical Research and Materiel Command
Fort Detrick, Maryland 21702-5012

REPORT DOCUMENTATION PAGE

Form Approved
OMB No. 0704-0188

1. REPORT DATE *(DD-MM-YYYY)*	**2. REPORT TYPE**	**3. DATES COVERED** *(From - To)*
01-07-2006	Final	16 JUN 2003 - 15 JUN 2006

4. TITLE AND SUBTITLE
The Antemortem Detection and Conformational Switches of Prion Proteins

5a. CONTRACT NUMBER

5b. GRANT NUMBER
DAMD17-03-1-0285

5c. PROGRAM ELEMENT NUMBER

6. AUTHOR(S)
David Schuber, Ph.D.

E-Mail: schubert@salk.edu

5d. PROJECT NUMBER

5e. TASK NUMBER

5f. WORK UNIT NUMBER

7. PERFORMING ORGANIZATION NAME(S) AND ADDRESS(ES)

Salk Institute for Biological Studies
La Jolla, CA 92037-1099

8. PERFORMING ORGANIZATION REPORT NUMBER

9. SPONSORING / MONITORING AGENCY NAME(S) AND ADDRESS(ES)
U.S. Army Medical Research and Materiel Command
Fort Detrick, Maryland 21702-5012

10. SPONSOR/MONITOR'S ACRONYM(S)

11. SPONSOR/MONITOR'S REPORT NUMBER(S)

12. DISTRIBUTION / AVAILABILITY STATEMENT
Approved for Public Release; Distribution Unlimited

13. SUPPLEMENTARY NOTES

14. ABSTRACT:

Blood from animals with prion disease contain low levels of prion infectivity, which primarily resides in the white blood cells (WBCs). We have developed a method that combines isolation of WBCs and cell blotting of PrPsc to detect individual cells that contain PrPsc. Sensitivity studies suggest that it can detect as low as 10 prion-infected cells in 5 x 105 WBCs. The assay is able to detect the prion-infected cells in the blood of some, but not all, prion-infected animals at the clinical stage. We believe that the combination of this method with a recently published successful cyclic amplification of protein misfolding (PMCA) procedure may give the required sensitivity for antemortem detection of prion in blood. In addition, a structure-activity relationship study of the fungal HET-s prion shows that a unique amyloid fibrillar structure is the infectious entity of the HET-s prion, and glycoform stoichiometry of host protein was found to regulate prion strain specificity.

15. SUBJECT TERMS

16. SECURITY CLASSIFICATION OF:			**17. LIMITATION OF ABSTRACT**	**18. NUMBER OF PAGES**	**19a. NAME OF RESPONSIBLE PERSON**
a. REPORT	**b. ABSTRACT**	**c. THIS PAGE**			USAMRMC
U	U	U	UU	40	**19b. TELEPHONE NUMBER** *(include area code)*

Table of Contents

Introduction

Prion diseases such as bovine spongiform encephalopathy (BSE) are threats to animals such as cattle, to food safety, and to humans that use biomedical products developed from animal sources. Prions are also potential biological warfare agents. Current methods for diagnosing prion diseases only work on postmortem material. A proven antemortem diagnostic or screening test is not yet available.

The amyloidogenic PrP^{Sc} is the only proven surrogate marker for the diagnosis of prion diseases. Therefore almost all of the efforts for diagnosing prion diseases are directed at detecting PrP^{sc}. Since the only difference between the normal cellular PrP^{c} and the pathological PrP^{sc} is their conformation, current methods distinguish them by taking advantage of their different physicochemical properties or by using antibodies that recognize PrP^{sc}. The most common techniques detect PrP^{sc} by its relative resistance to digestion by proteinase K, followed by amplification of the PrP^{sc} signal with Western blotting, ELISA, or fluorescence techniques using antibodies that recognize PrP (Bolton, 2001 and Borman, 2002). However, antibodies that only recognize PrP^{sc} are rare, and their usefulness is limited by species specificity. Currently available methods for prion diseases are sensitive enough for prion-enriched, postmortemly available tissues such as brain, but cannot detect the low levels of prions in body fluids such as blood that are readily available from living animals.

There is a solid foundation for developing an antemortem test with blood because there is strong evidence that blood taken from diseased animals contains prion infectivity (Aguzzi, 2000; Brown et al., 2001, Heikenwalder et al., 2005). Most of the infectivity resides in the "buffy coat" fraction that contains lymphocytes and mononuclear cells. Only a small fraction of the infectivity stays in the plasma that contains no cells. For example, it is reported that the blood infectivity level during the preclinical stage is 6 to12 infectious units (IU) per ml of buffy coat and only a trace amount of infectivity is in plasma. However, infectivity rises sharply to 100 IU/ml of buffy coat and 20 IU/ml of plasma at the onset of clinical signs (Brown et al., 1999). Despite this evidence, current methods have been unable to detect the small amount of PrP^{sc} in blood taken from infected animals. It is estimated that one IU contains as few as 10,000 molecules of PrP^{sc} (10^{-15} g), so a method capable of detecting 0.01 pg to 0.1 pg (10^{-14} g to 10^{-13} g) of PrP^{sc} is required. Urine collected from infected animals appears to be a better source than blood for antemortem prion detection. Shaked et al. (2001) found that a protease-resistant form of PrP^{sc} ($UPrP^{sc}$) could be detected with Western blotting in the urine of animals and humans suffering from TSE. Unfortunately, the promising discovery of protease-resistant PrP in urine could not be confirmed in later studies (Prusiner, 2004).

The initial aim of our research was to develop an antemortem test for prion diseases based on a non-immunological, cell-based biological assay for the detection of PrP amyloid species. In addition, we focused on elucidating the infectious entity of prions and the molecular mechanism of generating prion infectivity.

Towards the development of an antemortem prion test, we have previously developed a cell-based assay that can detect the β-sheeted aggregates or fibrils of amyloidogenic proteins. The assay is based on the ability of amyloidogenic proteins to induce a unique form of cellular MTT (3-(4,5-dimethylthiazol-2-yl)-2,5-diphenyltetrazolium bromide) formazan exocytosis (Liu et al, 1997 a&b; 1998 a&b; 1999 and 2001). During the first year of our research under this grant, individual prion-infected neuroblastoma cells were found to undergo amyloidogenesis that could be detected with the cell-based MTT formazan exocytosis assay. This phenomenon formed the foundation for developing a blood-based antemortem test by detecting prion-infected white blood cells (WBCs) with the cell-based MTT formazan exocytosis assay. The idea is that enrichment of prion-infected WBC subtypes by cell isolation techniques plus the detection of

individual infected cells with the cellular MTT formazan exocytosis assay may give the required sensitivity for antemortem detection of prions in blood. We investigated this idea thoroughly during the second year, and found that that the cellular MTT formazan exocytosis assay is not sensitive enough for detecting prion-infected blood cells because of the background problem with certain WBCs and the apparent high false negative rate of the assay. We then changed the detection method by combining WBC isolation and cell blotting of PrP^{sc} to detect individual cells that contain PrP^{sc}. A sensitivity study shows that as low as 10 to 50 prion-infected cells can be detected by this method, suggesting that it may have the potential to be used for the antemortem detection of prion infection in blood. In the third year, we further optimized this method and evaluated its sensitivity with prion-infected mouse blood. The progress was reported below.

Towards the elucidation of the mechanism of prion infectivity and its infectious entity, we determined the structure-activity relationship of the HET-s prion system of the filamentous fungus Podospora anserina. We studied the structure of the amyloid fibrils of the HET-s prion protein and showed by a mutagenesis approach that this conformation is the functional and infectious entity of the HET-s prion. These results correlate for the first time distinct structural elements with prion infectivity (Ritter et al., 2005). We also made new findings on the mechanism of prion strain specificity and in the *de novo* generation of prion infectivity from recombinant prion protein.

Body

1. Developing a blood-based antemortem test by detecting prion-infected white blood cells (WBCs) with the cell-based MTT formazan exocytosis assay.

We have previously developed a cell-based assay that can detect the β-sheeted aggregates or fibrils of amyloidogenic proteins. The assay is based on the ability of amyloidogenic proteins to induce a unique form of cellular MTT (3-(4,5-dimethylthiazol-2-yl)-2,5-diphenyltetrazolium bromide) formazan exocytosis (Fig. 1 A to C, also see Liu et al, 1997 a&b; 1998 a&b; 1999 and 2001). First we tested whether prion proteins, a class of proteins that are known to be amyloidogenic, also form the β-sheeted aggregates or fibrils that can be detected by cellular MTT formazan exocytosis. The fungal prion protein HET-s of *Podospora anserina* aggregates *in vitro* into infectious amyloid-like fibrils (Dos Reis et al., 2002; Maddelein et al., 2002). We also found that HET-s monomers aggregate to form protein fibrils *in vitro* that show Congo red birefringence, an indication that the protein fibrils are amyloid fibrils (Fig. 1D). To test whether HET-s enhances cellular MTT formazan exocytosis like other amyloid proteins, B12 cells were incubated with HET-s fibrils overnight. As shown in Fig. 1E and Table 1A, HET-s induced unique MTT formazan crystals which are morphologically identical to that induced by other amyloid proteins such as $A\beta_{1-42}$ (Fig. 1C). As a negative control, a HET-s protein sample denatured by trichloroacetic acid precipitation did not induce amyloid-like MTT formazan exocytosis (Fig. 1F and Table 1A). These results are an additional confirmation that enhancing cellular MTT formazan exocytosis is a common biological activity of all amyloid proteins.

To test whether amyloidogenesis occurs in prion-infected cells, N2a neuroblastoma cells infected with the RML strain of mouse prion (ScNB cells, Caughey and Race, 1992) were examined for amyloid-induced cellular MTT formazan exocytosis directly without any other treatment. Fig. 2B (arrows) and Table 1B show that approximately 13% of the cells (up to 30%) contained the characteristic amyloid-induced MTT formazan. N2A cells that were not infected with prion did not show this phenomenon (Fig. 2A). Treatment of the ScNB cells with 5 μM

Congo red for 3 days, a known inhibitor of PrP-res (PrP^{Sc}) accumulation (Caughey and Race, 1992), completely abolished amyloid-induced MTT formazan (Fig. 2C and Table 1B). Western blotting of PrP-res (PrP^{Sc}) in N2a cells, ScNB cells and ScNB cells treated with 5 µM Congo red for 3 days shows that amyloid-induced MTT formazan exocytosis is strictly correlated with the presence of PrP-res (PrP^{Sc}) (Fig. 2D). These results demonstrate that individual cells infected with prion can undergo amyloidogenesis and be detected by the cellular MTT formazan exocytosis assay.

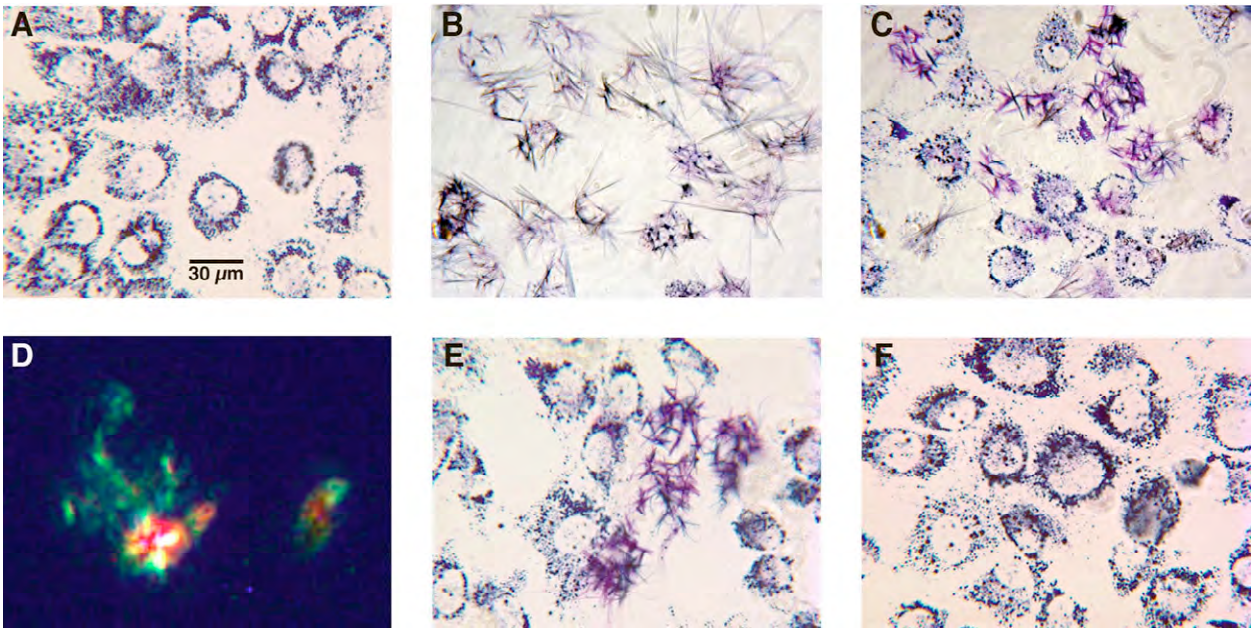

Fig. 1. The fungal prion protein HET-s aggregates into amyloid fibrils in vitro and induces amyloid-like cellular MTT formazan exocytosis. B12 cells were treated as indicated, followed by 30 min or 3 hr of MTT (0.5 mg/ml) reduction. **(A)** Control, 30 min MTT reduction. **(B)** Control, 3 hr MTT reduction. Note the morphology of the naturally occurring MTT formazan. **(C)** 1 µM $A\beta_{1-42}$ overnight incubation followed by 30 min MTT reduction. The MTT formazan crystals are thicker, shorter and purple. **(D)** Congo red bifringence of HET-s amyloid fibrils. **(E)** HET-s was buffer exchanged from 6 M Guanidinium chloride to 50 mM Tris pH 8.0, 1 mM dithiothreitol. B12 cells were incubated with 2 µM HET-s overnight followed by 30 min MTT reduction. **(F)** The same as in **(E)** except HET-s in 6 M Guanidinium chloride was first precipitated with trichloroacetic acid.

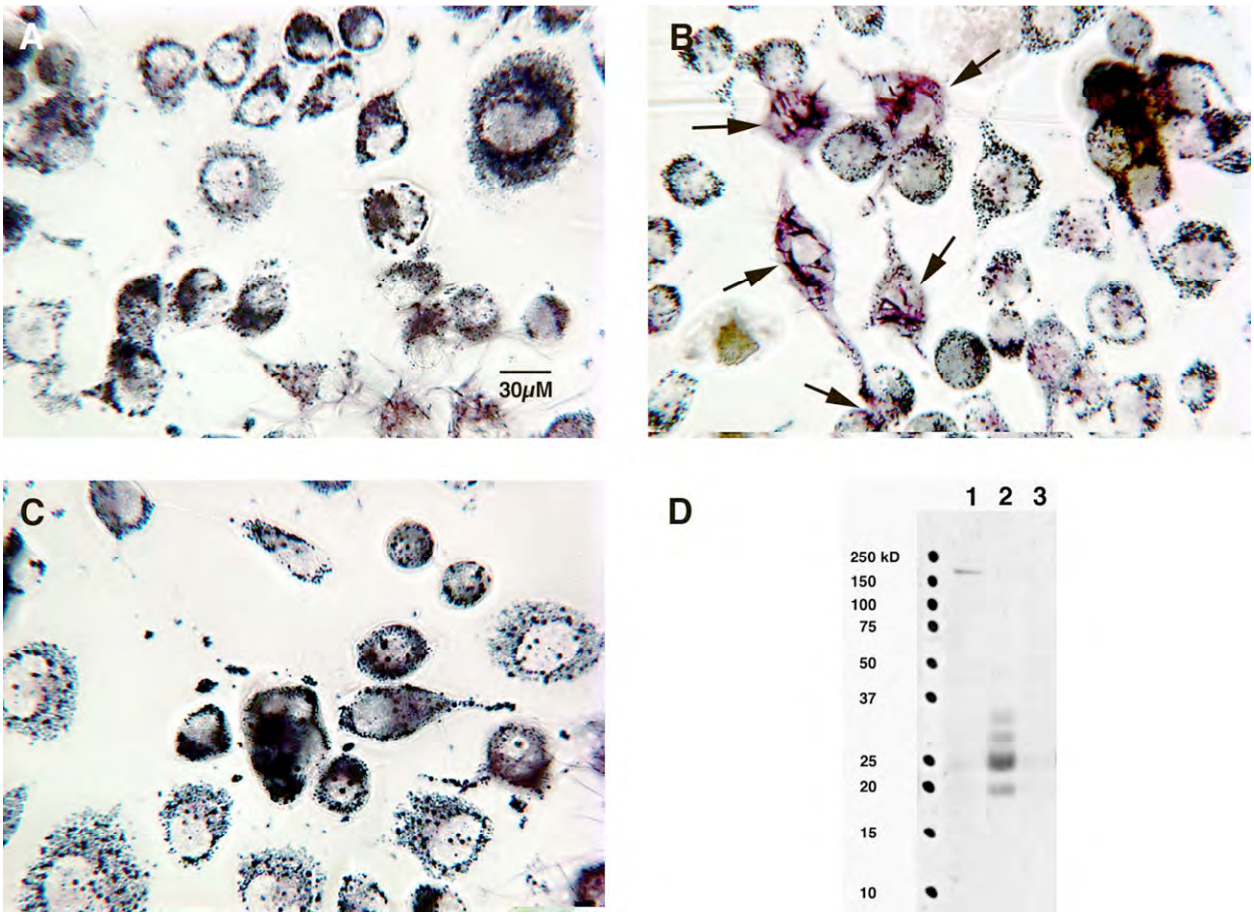

Fig. 2. Detection of amyloidogenesis in prion-infected neuroblastoma cells with cellular MTT formazan exocytosis. Normal N2a cells **(A),** ScNB cells **(B)** and ScNB cells treated with 5 μM Congo red for 3 days **(C)** were incubated with MTT (0.5 mg/ml) for 60 min at 37°C and imaged under a light microscope. Arrows indicate cells with amyloid-induced MTT formazan crystals. **(D)** Western blotting of PrP-res: Line **1**, normal N2a cells; Line **2**, ScNB cells; line **3**, ScNB cells treated with 5 μM Congo red for 3 days.

Table 1 Prion protein-induced MTT formazan exocytosis

Treatment	Percentage of cells showing amyloid-induced MTT formazan
A. Fungal prion protein HET-s	
Solvent control	**0**
1 μM $A\beta_{1-42}$	**33 ± 5***
2 μM HET-s	**21 ± 4***
2 μM denatured HET-s	**0**
B. Mammalian prion-infected N2a cells	
Normal N2a cells	**0**
ScNB cells	**13 ± 5***
ScNB cells + 5 μM Congo red for 3 days	**0 to 1**

The effect of HET-s on cellular MTT formazan exocytosis by B12 cells was carried out as described in the legend of Fig. 1. The effect of prion infection on the cellular MTT formazan exocytosis of N2a cells was described in the legend of Fig. 2. All data are mean ± S.D. of four experiments. *: Significantly different from solvent control or normal N2a cells.

The finding that individual neuroblastoma cells infected with prion can undergo amyloidogenesis and be detected with the MTT formazan exocytosis assay formed the foundation for developing a novel antemortem test by detecting prion-infected white blood cells (WBCs) with the cell-based MTT formazan exocytosis assay. Detecting the small numbers of infected WBCs among millions of blood cells with cell isolation techniques and the MTT formazan exocytosis assay could represent 100-fold of increase in detection sensitivity compared with other types of methods (e.g. Western or ELISA of buffy coat). Western blotting methods and ELISA assays typically requires more than 10^4 cells. The current understanding of the prion transmission process through the oral route is that the infectious agent first penetrates the intestinal mucosa through M cells and reaches Peyer's patches, and from there they are transported to lymphoreticular system (e.g. spleen and lymph nodes), possibly through myeloid dendritic cells (Huang et al., 2002). The prion then amplifies and accumulates in follicular dendritic cells and other unidentified cells of the lymphoreticular system. Finally, the prion reaches the peripheral nervous system and brain (Weissmann et al., 2002), possibly through transport by CD11c+ dendritic cells (Aucouturier et al, 2001). It is conceivable that some infected cells in the lymphoreticular system will be found in blood circulation during this transmission process, although the number may be few. There also appears to be a reverse propagation of prion infectivity from brain to the lymphoreticular system during the late stage of the disease, because there is a 5 to 10 fold increase in blood prion infectivity during the clinical stage of intracerebrally inoculated mice (Brown et al., 1999). Therefore, prion-infected WBCs should be present in blood circulation during both preclinical and clinical stages of the disease. Exactly what type of WBCs carries prion infectivity is not clear, although dendritic cells which have a higher expression of PrP^c are a primary suspect.

To use cellular MTT formazan exocytosis as a method for detecting prion-infected WBCs, two prerequisites need to be fulfilled. One is that the WBCs should respond to amyloid proteins in the MTT assay like the neuroblastoma cells, and the other is that prion-infected WBCs should have acquired or formed prion amyloid species. It is possible that not all prion-infected cells have formed or acquired prion amyloid species. In this case, a false negative will arise.

In initial studies, we isolated buffy coat from normal hamsters and mice. WBCs from both mice and hamster (not shown) reduced MTT like other cells tested (Fig. 3A), and responded to amyloid β peptide treatment with amyloid-type MTT formazan (Fig. 3B) while non Aβ-treated WBCs did not show amyloid-type MTT formazan (Fig. 3A).

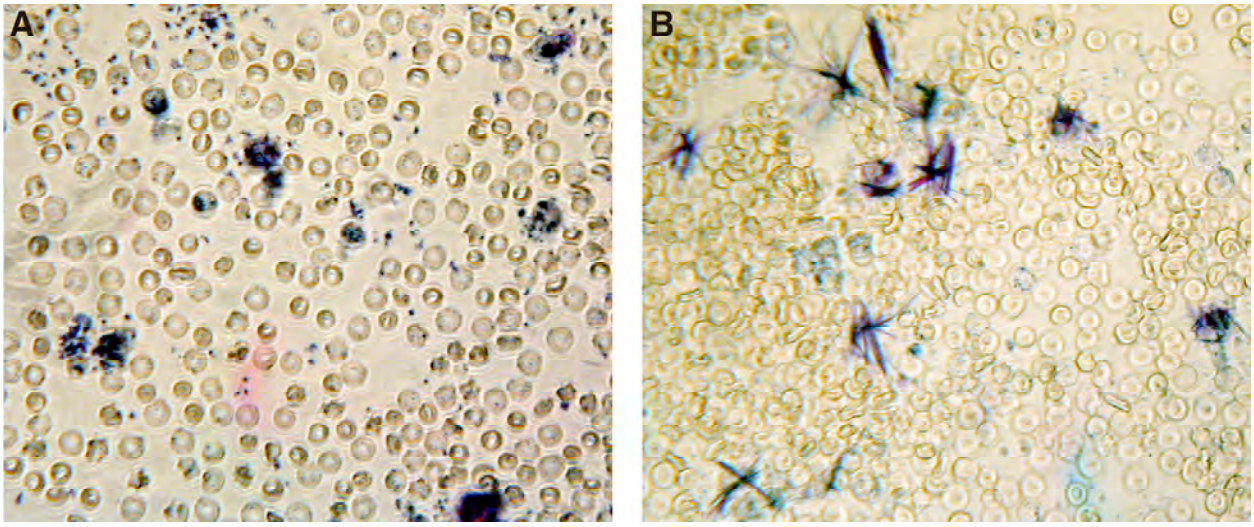

Fig. 3. Mouse blood WBCs reduce MTT and respond to Aβ treatment with characteristic amyloid-induced MTT formazan exocytosis. Buffy coat isolated from mouse blood (in RPMI 1640 medium plus 10% fetal calf serum, still contaminated with red blood cells and platelets) was treated with 5μM Aβ1-42 (B) or untreated (A) for 3 hr at 37°C, followed by 1 hr of MTT reduction (0.5 mg/ml).

To investigate more specifically the responsiveness of various types of WBCs to amyloid protein, we isolated T cells, B cells, monocytes and CD11c+ dendritic cells from mouse blood as well as mouse spleen, using cell-specific antibody-coated magnetic beads from Miltenyi Biotec (Auburn, CA). Various types of WBCs reduced MTT like other cells tested and responded to amyloid β peptide (Aβ) treatment with amyloid-type MTT formazan (Table 1). However, T cells showed a significant background (~5%) even in the absence of Aβ treatment, making detection of level infection difficult or impossible. Finally, CD11c+ dendritic cells showed a low response to Aβ (Table 2).

Table 2. Effects of Aβ on Cellular MTT Formazan Exocytosis by Various Types of Mouse WBCs

	Percent of cells with amyloid-induced MTT formazan	
Cell Type	**Untreated**	**Treated with 5 μM $A\beta_{1-42}$**
B cells	**1 ± 2**	**90 ± 5**
T cells	**5 ± 2**	**93 ± 4**
Monocytes	**0**	**92 ± 5**
CD11c+ dendritic cells	**0**	**33 ± 56**

Various types of WBCs were isolated from mouse spleen with Miltenyi's MACS magnetic beads coated with cell-specific antibody according to the manufacture's procedures. The cell-specific

microbeads are CD19 for B cells, CD90 for T cells, CD11b for monocytes, and CD11c for dendritic cells. The cells were treated with 5μM $A\beta_{1-42}$ or untreated for 5 hr at 37°C, followed by 1 hr of MTT reduction (0.5 mg/ml). Data are the mean ± S.D. of three experiments.

The other concern is the percentage of prion-infected cells that can be detected by the MTT formazan exocytosis assay. By subcloning and subsequent detection of PrP^{sc} by Western blotting in subclones of prion-infected mouse neuroblastoma cells, Caughey and collegues at NIH's Rock Mountain Laboratory found that up to 90% of cells in the original cell line are infected (Caughey et al., unpublished results). In contrast, the cellular MTT formazan exocytosis only detected up to 30% of the infected cells from this cell line. These findings suggest that only a certain percentage of prion-infected cells can form amyloid species that can be detected by the MTT formazan exocytosis assay. However, in another model system of prion infectivity, we showed that the amyloid fibrillar conformation of the fungal HET-s prion is the infectious entity in P. anserina (see below) and that amyloid fibrils of HET-s can be detected by the MTT formazan exocytosis assay.

In summary, these results suggest that the cellular MTT formazan exocytosis assay is an interesting method for basic research of amyloid proteins, but it is not sensitive enough for detecting prion-infected blood cells because of the background problem with certain WBCs and the apparent high false negative rate of the assay.

2. Developing a blood-based antemortem test by detecting prion-infected WBCs with cell isolation and cell blotting of PrP^{sc}

Because of the background problem and the high false negative rate, the original idea of using the amyloid-induced MTT phenomenon to detect prion in blood was abandoned. However, the idea of increasing detection sensitivity by looking at individual blood cells instead of pooled cells is still a promising one. So far the only proven surrogate marker for the diagnosis of prion diseases is PrP^{Sc}. By detecting PrP^{Sc}, one would be able to avoid the false negative rate and the cell responsiveness problem associated with the cellular MTT formazan exocytosis assay. A technique that allows the detection of PrP^{Sc} in individual cells is the cell blotting method developed for prion-infected cell lines (Bosque and Prusiner, 2000; Klohn et al., 2003). We therefore tried to adopt this technique to blood cells. Theoretically, trying to detect individual blood cells containing PrP^{Sc} through cell blotting could increase sensitivity by 100 to 1000 times when compared with Western blotting for PrP^{Sc}. It may be possible to identify the small number of prion-infected cells in blood by this technique.

1) *Isolation of WBCs from blood.* We chose mouse as the experimental animal since prion-infected blood was available to us for the development of the method. The total volume of blood obtainable from a mouse is between 0.5 ml to 1 ml per mouse. The total number of WBCs in such volume of blood was found to be 0.5 to 1 million. Although one can isolate specific type of WBCs with magnetic beads (such as dendritic cells), it is better to use the entire WBCs for prion detection since the type(s) of WBCs that carry PrP^{Sc} is not certain at present time. Using the entire WBCs for prion detection will also simplify the procedure and detect PrP^{Sc} in both cells that amplify PrP^{Sc} and cells that acquired PrP^{Sc} without assuming which type of cells are infected. We used a two-step OptiPrep density gradient method to isolate WBCs by first getting rid of the red blood cells (RBCs), and then the platelets.

2) *Cell blotting of WBCs.* We found that a cytocentrifuge (StatSpin Cytofuge 2, MA) is good for spreading and depositing the WBCs onto a microscope slide so that signal from individual cells can be detected. The WBCs deposited on a microscope slide were then blotted

to a nitrocellulose membrane as described by Bosque and Prusiner (2000) and Klohn et al. (2003). Briefly, the blot was air-dried for 1 hr at 37°C, rewetted in lysis buffer (50 mM Tris HCl pH 8.0, 150 mM NaCl, 0.5% sodium deoxycholate, and 0.5% Triton X-100), and incubated in lysis buffer with 5 µg/ml proteinase K at 37°C for 90 min with constant shaking. Next, the blot was washed twice with distilled water and incubated with 2 mM AEBSF (Roche Applied Science) for 10 min at room temperature to inactivate proteinase K. The membrane was then incubated in denaturing buffer (3 M guanidinium thiocyanate, 10 mM Tris HCl, pH 8.0) for 10 min, washed 3 times with water and blocked with 5% nonfat dry milk in Tris-buffered saline with 0.1% Tween-20 (TBST) for 1 hr at room temperature. The blot was next incubated with anti-PrP Fab HuM-D18 (1:1000, InPro Biotechnology, San Francisco) in TBST-5% BSA for 1 hr at room temperature or overnight at 4°C, washed 3 times with TBST, then incubated with horseradish peroxidase-conjugated goat anti-human IgG $F(ab')_2$ (Pierce, 1:20,000, in TBST-5% nonfat dry milk) for 1 hr at room temperature. After washing 4 times, the signal was detected with the Super Signal West Pico ECL kit (Pierce) and x-ray film (Hyperfilm ECL, GE Healthcare). The cell blotting procedure can be carried out in one day and can be automated (Klohn et al., 2003)

3) *The sensitivity of the cell blotting technique.* We first learned the technique of cell blotting by using prion-infected neuroblastoma cell line ScN2A (from Dr. Byron Caughey at NIH's Rock Mountain Lab) and ScGT1-trk (InPro Biotechnology), and then determined the sensitivity of the cell blotting technique. Assuming ScGT1-trk cells are 100% prion-infected, we added sequentially decreasing numbers of ScGT1-trk cells (1000 cells, 500 cells, 100 cells, 50 cells, 10 cells) to 5 x 10^5 mouse WBCs and then went through the cell blotting procedure. As shown in Fig. 4, as low as 50 prion-infected cells can be reliably detected. By optimizing the protease K digestion step, it was found that as low as 10 prion-infected cells 5 x 10^5 WBCs can be reliably detected and differentiated from background (Fig. 5). These results suggest that it is possible that the low number of prion-infected cells in blood can be detected by the WBCs isolation plus the cell blotting approach.

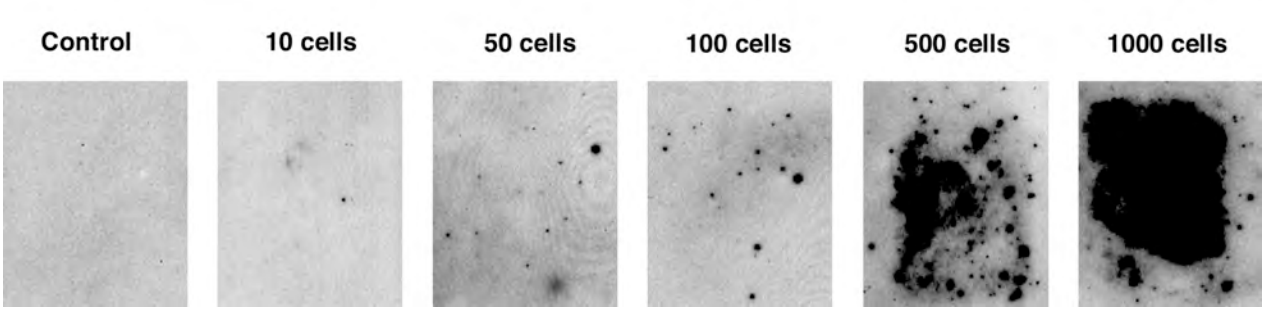

Fig. 4. The sensitivity of the cell blotting technique. Different numbers of ScGT1-trk cells (0 cell=control, 10 cells, 50 cells, 100 cells, 500 cells, and 1000 cells) were added to 5 x 10^5 mouse WBCs and then processed through the cell blotting procedure as described above.

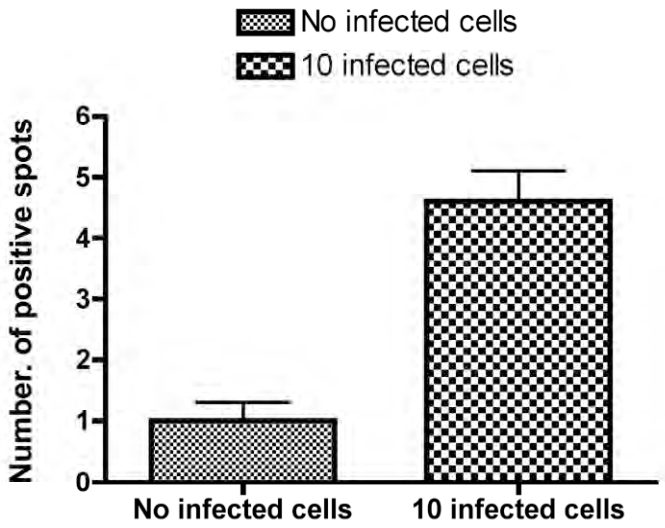

Fig. 5. The sensitivity of the cell blotting technique. Zero or 10 prion-infected ScGT1-trk cells were added to 5 x 10^5 mouse WBCs and then processed through the cell blotting procedure as described above except the protease K digestion step was modified to 3 µg/ml proteinase K at 37°C for 60 min. Data are the mean ± S.D. of five experiments.

4) *Application of the cell blotting method to WBCs from blood of prion-infected mice.* Our procedure requires freshly drawn blood from prion-infected animals. Because of this limitation, and despite much effort, we were only able to obtain blood from a limited number of prion-infected animals to evaluate the sensitivity and specificity of the method. As shown in Table 3, the method is specific in that the PrP^{Sc}–positive spots are never above background level in the blood of a large number of control animals. In 4 blood samples from mice that have been infected with the RML strain of mouse prion and have reached the clinical stage, one is definitely positive as judged by the assay, one lies in the boarderline of positive/background, and two are not above background. These results suggest that the assay is able to detect the prion-infected cells in the blood of some, but not all, prion-infected animals at the clinical stage.

Table 3. Detection of PrP^{Sc} in mouse blood with WBC isolation/cell blotting

Blood type	Number of PrP^{Sc}-positive spots
Control animals, n=10	1 ± 0.7
Prion-infected animals:	
Animal #1	8
Animal #2	3
Animal #3	2
Animal #4	2

Number of PrP^{Sc}-positive spots in the blood samples were determined as described above. Data are the mean ± S.D. for the control animals.

3. The detection of PrP^{Sc} molecules in blood by a combination of cyclic amplification of protein misfolding (PMCA) and the cell-based assay

In the *The Statement of Work* of our original grant application, we proposed to detect PrP^{Sc} molecules in blood by a combination of cyclic amplification of protein misfolding (PMCA) and the cell-based assay. However, despite much effort, the maximum amplification of PrP^{Sc} molecules we could achieve through PMCA was 3 to 10 times, not the over 60 times as reported (Saborio et al., 2001). This line of research was therefore abandoned. Recently, Soto and colleagues (Castilla et al., 2005) have developed a modified PMCA procedure with automated sonication, which allows many more cycles of amplification and 140 PMCA cycles leads to a 6,600-fold increase in sensitivity over standard detection methods. Two successive rounds of PMCA resulted in a 10-million-fold increase in sensitivity and a capability to detect as little as 8,000 molecules of PrP^{Sc}. Remarkably, they found that serial PMCA enables detection of PrP^{Sc} in blood samples of prion-infected hamsters with 89% sensitivity and 100% specificity. These new findings, if confirmed, essentially solved the problem of prion detection in the blood of infected animals. By combining the successful PMCA procedure from these authors with the WBC isolation/cell blotting procedure described in this report, it is possible to further increase the detection sensitivity, solving the problem of antemortem detection of infectious prion in blood.

4. Correlation of structural elements and infectivity of the HET-s prion

Prions are believed to be infectious, self-propagating polymers of otherwise soluble, host-encoded proteins. This concept is now strongly supported by the recent findings that amyloid fibrils of recombinant prion proteins from yeast*, Podospora anserina* and mammals can induce prion phenotypes in the corresponding hosts. However, the structural basis of prion infectivity remained largely elusive because acquisition of atomic resolution structural properties of amyloid fibrils represents a largely unsolved technical challenge. HET-s, the prion protein of *P. anserina*, contains a carboxy-terminal prion domain comprising residues 218–289. Amyloid fibrils of HET-s(218–289) are necessary and sufficient for the induction and propagation of prion infectivity. We have used fluorescence studies, quenched hydrogen exchange NMR and solid state NMR to determine the sequence-specific positions of amyloid fibril secondary structure elements of HET-s(218–289). This approach revealed four β-strands constituted by two pseudo-repeat sequences, each forming a β-strand-loop-β-strand motif (Fig. 6). By using a structure-based mutagenesis approach, we show that this conformation is the functional and infectious entity of the HET-s prion. These results correlate distinct structural elements with prion infectivity.

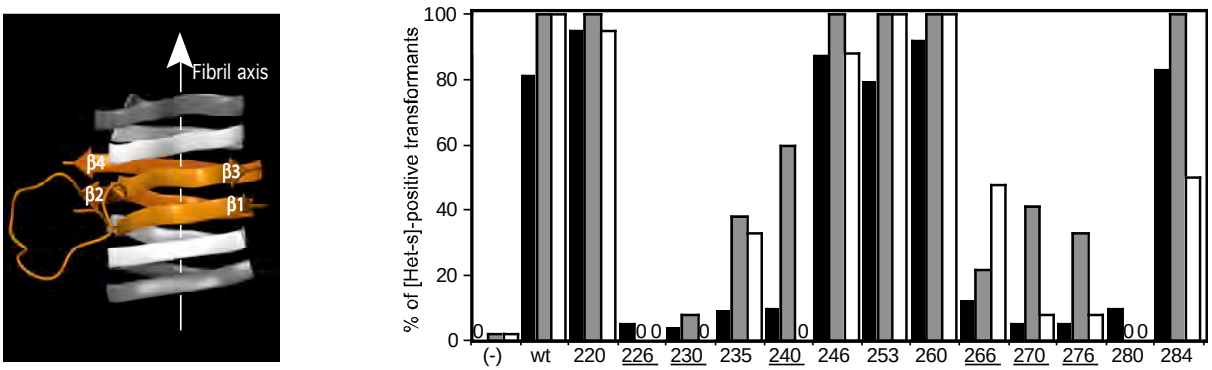

Fig. 6. The Fold of the HET-s(218-289) fibrils is infectious. (Left) The proposed fold is shown comprising two pseudo-repeat sequences, each forming a beta-strand-loop-beta-strand motif. (Right) In vivo prion formation of Het-s proline point mutants (for example P220, P226, …) introduced into a knock-out Het-s P. anserina strain. Given are the percentage of transformants producing a cell death reaction when confronted with a het-s tester colony (black columns), and the percentage of transformants displaying infectivity immediately after infection (grey columns) and after a 3-day subculture (white columns).

5. Glycoform Stoichiometry of Host Protein Regulates Prion Strain Specificity

Different "strains" of infectious prions maintain unique pathological and biochemical features upon serial passage. In Collaboration with S. Supattapone (Dartmouth Medical School, Hanover), we showed that N-linked glycosylation controls the ability of the normal mammalian prion protein (PrP^C) to be converted into its pathogenic conformation (PrP^{Sc}) in a strain-dependent manner. Strikingly, unglycosylated PrP^C molecules are required to propagate RML prions, whereas diglycosylated PrP^C molecules are required to propagate Sc237 prions. These results provide the first direct evidence that the stoichiometry of host-encoded PrP^C glycoforms influences the strain specificity of prion propagation. Since this work has not been published yet, we will describe it in more details.

Recent biophysical studies of model proteins suggest that the formation of prion strains may be governed by differences in the potential folding pathways available to different protein substrates. Therefore, we decided to investigate whether the glycosylation profile of PrP^C molecules affects their ability to interact with different prion strains. Towards this aim, we used a direct biochemical approach to produce and isolate natively processed, wild type PrP^C glycoforms and then used the Protein Misfolding Cyclic Amplification (PMCA) technique to test the ability of isolated PrP^C glycoforms, alone and in combination, to amplify and propagate purified PrP27-30 PrP^{Sc} molecules derived from different prion strains.

Using Cu^{2+}-affinity and ion exchange chromatography, we first purified PrP^C from either mouse or hamster brains to produce a "native" preparation of the normal distribution of PrP^C molecules in whole brain for each species (Fig. 7A, lane 1). We performed PMCA reactions in the presence of $Prnp^{0/0}$ (Abl) brain homogenate. The "native" preparation of mouse PrPc successfully amplified PrP^{Sc} molecules derived from RML, and the "native" preparation of hamster PrP^C amplified PrPSc molecules fromSc237 (Fig. 7A, lanes 7-9). We also produced an unglycosylated PrP^C substrate, designated "UN," by enzymatically deglycosylating the purified, "native" PrP^C preparation with N-glycosidase F (PNGase F) under non-denaturing conditions, and then re-purifying the digested product (Fig. 7A, lane 2). In PMCA reactions, unglycosylated mouse PrP^C substrate successfully amplified RML PrP^{Sc} template in the presence of Abl brain homogenate (Fig. 7A, top panel, lane 11), indicating that N-linked glycosylation of PrP^C is not required for RML prion conversion. In contrast, the unglycosylated

hamster PrP^C substrate did not amplify Sc237 PrP^{Sc} template under similar conditions (Fig. 7A, bottom panel, lane 11). This unexpected result indicates that the ability of unglycosylated PrP^C molecules to undergo prion conversion depends upon the strain properties of the template PrP^{Sc} molecule.

Next, we sought to test the strain-specificity of other PrP^C glycoforms, either alone or in combination, for prion conversion by PMCA in the presence of Abl brain homogenate. To prepare PrP^C substrates with various glycoform profiles, we applied "native" PrP^C preparations of each species to an immobilized lectin column in the presence of 0.75 M NaCl. The flow-through fraction of the lectin column, designated "ALL," contained a nearly even distribution of di-, mono-, and unglycosylated PrP^C molecules (Fig. 7B, lane 2). Subsequent elution of the column with N-acetyl glucosamine yielded a preparation of predominantly diglycosylated PrP^C molecules, which we termed "DI" (Fig. 7B, lane 3). We then used PNGase F to deglycosylate the "DI" sample, producing an unglycosylated PrP^C preparation directly derived from "DI," which we termed "DI➔UN" (Fig. 7B, lane 4). Remarkably, isolated "DI" PrP^C substrate failed to amplify RML PrP^{Sc} template (Fig. 7B, top panel, lane 8), but deglycosylation of this preparation rescued the ability of "DI➔UN" PrP^C substrate to convert into RML PrP^{Sc} (Fig. 7B, top panel, lane 9). The inability of the "DI" PrP^C preparation to amplify RML PrP^{Sc} template indicates that the presence of unglycosylated PrP^C molecules within the "native" PrP^C preparation is required for conversion of the glycosylated isoforms. This surprising conclusion was confirmed by the observation that the "ALL" substrate containing all three mouse PrP^C glycoforms successfully formed RML PrP^{Sc}, including an isoform corresponding to diglycosylated PrP^{Sc} (Fig. 7B, top panel, lane 7). In marked contrast, isolated diglycosylated hamster PrP^C substrate successfully amplified Sc237 PrP^{Sc} template, showing that the presence of unglycosylated PrP^C molecules are not required for Sc237 PrP^{Sc} amplification (Fig. 7B, bottom panel, lane 8). Furthermore, the "ALL" substrate containing all three hamster PrP^C glycoforms did not amplify the Sc237 PrP^{Sc} template efficiently, indicating that unglycosylated PrP^C molecules competitively inhibit Sc237-induced conversion of glycosylated PrP^C molecules (Fig. 7B, bottom panel, lane 7).

Our results led us to hypothesize that the stoichiometric composition of PrP^C glycoforms controls the prion strain specificity of a multimeric substrate complex, and that there are functional interactions between different PrP^C glycoforms within such a complex. To test this hypothesis directly, we mixed isolated diglycosylated and unglycosylated PrP^C molecules together at various stoichiometric ratios, and then tested the ability of these mixtures to serve as substrates in PMCA reactions. These reconstitution experiments confirmed that unglycosylated

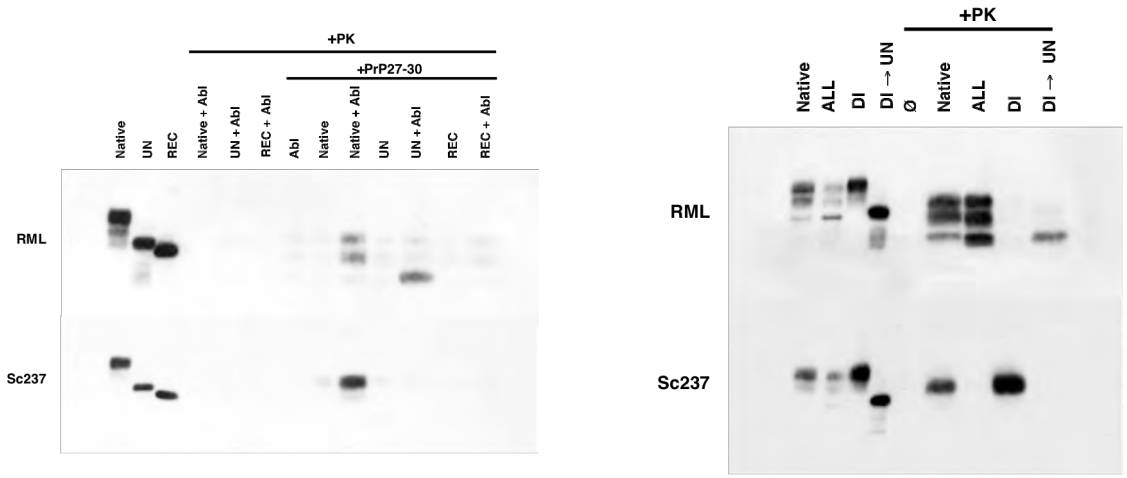

Fig. 7. Strain-dependent conversion of various PrP substrates. (Left) Western blot of PMCA reactions. Lanes 1-3: input substrates not treated with protease; lanes 4-12: each of the substrates indicated were subjected to PMCA in the absence (lanes 4-6) or presence (lanes 7-12) of PrP27-30 template. Abbreviations: Native = native PrP^C; UN = unglycosylated PrP^C; REC = recombinant PrP 23-231; Abl =

$Prnp^{0/0}$ brain homogenate. (Right) Western blot of PMCA reactions. Lanes 1-4: input samples not treated with protease; lanes 5-9: each of the substrates indicated were subjected to PMCA with PrP27-30 template in the presence of 5% Abl brain homogenate. Abbreviations: Ø = no substrate added; DI→UN = unglycosylated PrP^C prepared by deglycosylation of the DI preparation. RML = mouse substrates and RML template; Sc237 = hamster substrates and Sc237 template.

PrP^C molecules are required for amplification of RML PrP^{Sc} template; a 1:3 molar ratio of UN:DI was sufficient to drive formation of both PrP^{Sc} glycoforms (data not shown). In contrast, diglycosylated PrP^C molecules were required for the amplification of Sc237 PrP^{Sc} template. An approximately equimolar ratio of UN:DI PrP^C molecules was required to form Sc237 PrP^{Sc} *in vitro* (data not shown). To investigate further the effect of unglycosylated PrP^C molecules on the formation of Sc237 PrP^{Sc} molecules *in trans*, we performed an experiment in which a fixed concentration of hamster DI substrate was mixed with increasing concentrations of unglycosylated hamster PrP^C. Remarkably, the results indicate that unglycosylated PrP^C molecules dominantly inhibited the formation of diglycosylated Sc237 PrP^{Sc} molecules in a dose-dependent manner (data not shown). Similar studies with recombinant PrP molecules show that recombinant PrP resemble unglycosylated PrP^C molecules in their ability to inhibit *in vitro* amplification of Sc237 but not RML PrP^{Sc} template.

6. The failure to generate de novo infectivity from recombinant PrP converted into amyloid fibrils

According to the "protein only" hypothesis, the infectious agent of transmissible spongiform encephalopathy (TSE) is an alternative β-sheet rich conformation of the prion protein, PrP^{Sc}. However, the *de novo* generation of the TSE-agent starting from non-infectious recombinant prion protein was documented only once by the Prusiner group (Legname et al., 2004). A crucial step towards this aim is the generation of recombinant PrP that has the physicochemical characteristics of PrP^{Sc}. We established a conversion protocol originated by Luhrs in our lab, which generated recombinant PrP fibrils that comprise all the physicochemical characteristics of PrP^{Sc}. We then inoculated the recombinant material using various protocols in collaboration with Dr. M. Klein in Germany into Tg20 mice and never observed infectivity.

7. Expression of recombinant PrP in insect cells

Based on the observation that recombinant PrP fibrils are not infectious and the above studies in collaboration with S. Supattapone, we reasoned that either the glycosylation or/and the GPI anchor might be important prerequisites for the generation of PrP infectivity. Hence, we initiated the expression of GPI-anchored and glycosylated PrP in insect cells using the bacculovirus system. Preliminary expression tests are promising. GPI-free PrP as a GST-fusion protein is expressed and secreted to the medium (data not shown). GPI-PrP as a GST fusion protein is expressed and present in the cell pellet (Fig. 8).

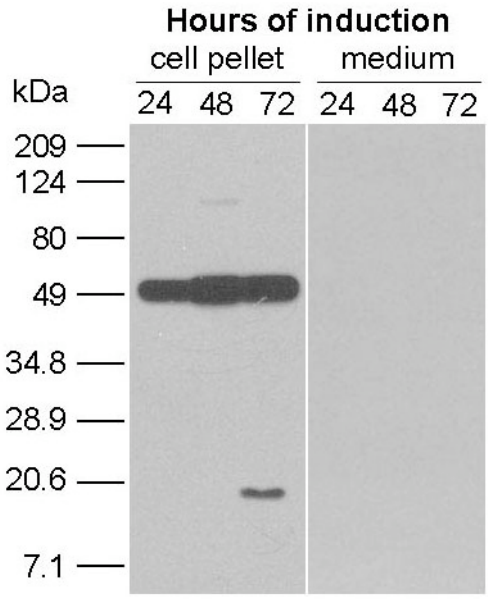

Fig. 8 Western Blot of Sf9 insect cells at different time points after infection with PrP-GPI Bacculovirus. The PrP signal was detected using the 6H4 monoclonal antibody, which detects prion proteins with very high specificity. The main band is observed near 49 kDa corresponding to the GST-PrP fusion protein. As can be seen significant amounts of PrP was present in the cell pellet already after 24 h after infection, and the maximum expression level was reached after 48 h. After 72 h some degradation was observed. In contrast, no PrP was detected in the corresponding volumes and time points of the supernatant. This indicates that all expressed PrP stays attached to the cell.

Key Research Accomplishments

- A method for identifying individual prion-infected white blood cells (WBCs) has been developed. The method employs WBCs isolation and cell blotting of PrP^{sc}. Sensitivity studies suggest that it can detect as low as 10 prion-infected cells in 5 x 10^5 WBCs. the assay is able to detect the prion-infected cells in the blood of some, but not all, prion-infected animals at the clinical stage.
- Prion proteins such as the fungal prion protein HET-s and mouse prion protein, like other amyloidogenic proteins, were found to form bioactive species that can be cellular MTT formazan exocytosis.
- Prion-infected cells were found to undergo amyloidogenesis in tissue culture condition.
- A structure-activity relationship of the HET-s prion is established. It shows that a unique amyloid fibrillar structure is the infectious entity of the HET-s prion.
- New results provide the first direct evidence that the stoichiometry of host-encoded PrP^C glycoforms influences the strain specificity of prion propagation.
- Successfully expressed recombinant PrP in insect cells, which makes it possible to study the role of glycosylation or/and the GPI anchor in the formation of *de novo* infectivity from recombinant PrP.

Reportable Outcomes

1. A manuscript entitled “Amyloidogenesis in prion-infected cells” (Neuroscience Letters, in press) is attached as Appendix 1.

2. A paper entitled “Correlation of structural elements and infectivity of the HET-s prion” published in Nature (Ritter C, Maddelein M-L, Siemer AB, Luhrs T, Ernst M, Meier BH, Saupe SJ, and Riek R. 435, 844-848, 2005) is attached as Appendix 2.

3. A meeting abstract entitled “The antemortem detection of prion proteins “ is attached as Appendix 3.

4. A manuscript in preparation that explains strain specificity of prion infectivity at a molecular level.

Conclusions

- WBCs isolation plus the cell blotting of PrP^{Sc}, if combined with successful PMCA procedure, may give the required sensitivity for antemortem detection of prion in blood.
- Prion proteins such as the fungal prion protein HET-s and mouse prion protein, like other amyloidogenic proteins, form bioactive species that can be cellular MTT formazan exocytosis.
- Prion-infected cells can undergo amyloidogenesis in tissue culture conditions.
- The amyloid conformation is the infectious entity in the HET-s prion.
- The stoichiometry of host-encoded PrP^{C} glycoforms influences the strain specificity of prion propagation.

References

Aguzzi, A. (2000) Prion diseases, blood and the immune system: concerns and reality. *Haematologica* 85, 3-10.

Aucouturier, P., Geissmann, F., Damotte, D., Saborio, G.P., Meeker, H.C., Kascsak, R., Carp, R.I., and Wisniewski, T. (2001) Infected splenic dendritic cells are sufficient for prion transmission to the CNS in mouse scrapie. J. Clin. Invest. 108, 703-708.

Bosque, P.J. and Prusiner, S.B. (2000) Cultured cell sublines highly susceptible to prion infection. *J. Virol.* 74, 4377-4386.

Bolton, D.C. (2001) Prions and proteins: distinguishing between conformations. *Lancet* 358, 171-180.

Borman, S. (2002) Prion diagnostics continue to advance. *Chemical & Engineering News* 80 (17), 27-28

Brown, P., Cervenakova, L., McShane, L.M., Barber, P., Rubenstein, R., and Drohan, W.N. (1999) Further studies of blood infectivity in an experimental model of transmissible spongiform encecphalopathy, with an explanation of why blood components do not transmit Creutzfeld-Jakob disease in humans. *Transfusion* 39, 1169-1178.

Brown, P, Cervenakova, L., and Diringer, H. (2001) Blood infectivity and the prospects for a diagnostic screening test in Creutzfeldt-Jakob disease. *J. Lab. Clin. Med.* 137, 5-13.

Baron, G.S., Wehrly, K., Dorward, D.W., Chesebro, B., Caughey, B. (2002) Conversion of raft associated prion protein to the protease-resistant state requires insertion of PrP-res (PrP(Sc)) into contiguous membranes. *EMBO J.* 21, 1031-1040.

Castilla , J., Saa, J., and Soto, C. (2005) Detection of prion in blood. *Nat. Med.* 11, 982-985.

Caughey, B.W., Dong, A., Bhat, K.S., Ernst, D., Hayes, S.F. and Caughey, W.S. (1991) Secondary structure analysis of the scrapie-associated protein PrP 27-30 in water by infrared spectroscopy. *Biochemistry*. 30, 7672-7680.

Caughey, B. and Race, R.E. (1992) Potent inhibition of scrapie-associated PrP accumulation by Congo red. *J. Neurochem.* 59, 768-771.

DeArmond, S.J., McKinley, M.P., Barry, R.A., Braufeld, M.B., McColloch ,J.R., and Prusiner, S.B. (1985) Identification of prion amyloid filaments in scrapie-infected brain. *Cell* 41, 221-235.

Dos Reis, S., Coulary-Salin, B. , Forge, V., Lascu, I., Begueret, J., and Saupe, S.J. (2002) The HET-s prion protein of the filamentous fungus Podospora anserina aggregates in vitro into amyloid-like fibrils. *J Biol. Chem.* 277, 5703-5706.

Heikenwalder, M., Zeller, N., Seeger, H., Prinz, M., Klohn, P.C., Schwarz, P., Ruddle, N.H., Weissmann, C., Aguzzi, A. (2005) Lymphocytic inflammation specifies the organ tropism of prions. *Science* 307, 1107-1110.

Huang, F.-P., Farquhar, C.F., Mabbott, N.A., Bruce, M.E., and MacPherson, G.G. (2002) Migrating intestinal dendritic cells transport PrPSc from the gut. *J. General Virology* 83, 267–271.

Kitamoto, T,, Tateishi, J,, Tashima, T,, Takeshita, I., Barry, R.A., DeArmond, S.J., Prusiner, S.B. (1986) Amyloid plaques in Creutzfeldt-Jakob disease stain with prion protein antibodies. *Ann. Neurol.* 20, 204-208.

Klohn, P.-C., Stoltze L., Flechsig, E., Enari, M., and Weissmann, C. (2003) A quantitative, highly sensitive cell-based assay for mouse scrapie prions. *Proc. Natl. Acad. Sci. USA* 100, 11666-11671.

Liu, Y. and Piasecki, D. (2001) A cell-based method for the detection of nanomolar concentrations of bioactive amyloid. *Anal. Biochem.* 289, 130-136.

Liu, Y. (1999) Understanding the biological activity of amyloid proteins in vitro: from inhibited cellular MTT reduction to altered cellular cholesterol homeostasis. *Prog. Neuro-Psychopharmacol. & Psychiat.* 23, 377-395.

Liu, Y,, Peterson, D., and Schubert, D. (1998a) Amyloid β peptide alters intracellular vesicle trafficking and cholesterol homeostasis. *Proc. Natl. Acad. Sci. USA* 95, 13266-13271.

Liu, Y. and Schubert, D. (1998b) Steroid hormones block amyloid fibril-induced MTT formazan exocytosis: relationship to neurotoxicity. *J. Neurochem.* 71, 2322-2329.

Liu, Y. and Schubert, D. (1997b) Cytotoxic amyloid peptides inhibit cellular MTT reduction by enhancing MTT formazan exocytosis. *J. Neurochem.* 69, 2285-2293.

Liu, Y,, Peterson, D., Kimura, H. and Schubert, D. (1997a) The mechanism of cellular MTT reduction. *J. Neurochem.* 69, 581-593.

Maddelein, M.L., Dos Reis, S., Duvezin-Caubet, S., Coulary-Salin, B., Saupe, S.J. (2002) Amyloid aggregates of the Het-s prion protein are infectious. *Proc. Natl. Acad. Sci.* 91, 648-656.

Nishina, K., Deleault, N.R, Lucassen, R.W., and Supattapone, S. (2004) In vitro prion protein conversion in detergent-solubilized membranes. *Biochemistry* 43, 2613-2621.

Pan, K,M,, Baldwin, M., Nguyen, J,. Gasset, M., Serban, A., Groth, D., Mehlhorn, I., Huang, Z., Fletterick, R.J., Cohen, F.E., and Prusiner, S.B. (1993) Conversion of alpha-helices into beta-sheets features in the formation of the scrapie prion proteins. *Proc Natl Acad Sci U S A* 90, 10962-10966.

Prusiner, S.B., McKinley, M.P., Bowman, K.A., Bolton, D.C., Bendheim, P.E., Groth, D.F., Glenner, G.G. (1983) Scrapie prions aggregate to form amyloid-like birefringent rods. *Cell* 35, 349-358.

Prusiner, S.B., (1998). Prions. *Proc. Natl. Acad. Sci. USA,* 95, 13363-83.

Prusiner, S.B., (2004) Detecting mad cow disease. *Scientific America* July issue, page 86-93.

Ritter, C., Maddelein, M.-L., Simer, A.B., Luhrs, T., Ernst, M., Meier, B.H., Saupe, S., Riek, R. (2005) Correlation of structural elements and infectivity of the HET-s prion. Nature. 435, 844-848.

Saborio, G.P., Permanne, B. and Soto, C. (2001) Sensitive detection of pathological prion protein by cyclic amplification of protein misfolding. *Nature*. 411, 810-813.

Safar, J., Wille, H., Itri, V., Groth, D., Serban, H., Torchia, M., Cohen, F.E., Prusiner SB. (1998) Eight prion strains have PrP(Sc) molecules with different conformations. *Nat. Med.* 4, 1157-1165.

Shaked, G,M,, Shaked, Y., Kariv-Inbal, Z., Halimi, M., Avraham, I., Gabizon, R. (2001) A protease-resistant prion protein isoform is present in urine of animals and humans affected with prion diseases. *J. Biol. Chem.* 276, 31479-31482.

Supattapone, S. (2004) Prion protein conversion in vitro. *J. Mol. Med.* 82, 348-355.

Wadsworth, J.D., Joiner, S., Hill, A.F., Campbell, T.A., Desbruslais, M., Luthert, P.J., Collinge, J. (2001) Tissue distribution of protease resistant prion protein in variant Creutzfeldt-Jakob disease using a highly sensitive immunoblotting assay. *Lancet* 358(9277), 171-180.

Weissmann, C, EnarI, M., Klohn, P.C., RossI, D., and Flechsig, E. (2002) Transmission of prions. *Proc. Natl. Acad. Sci. USA,* 99, 16378-16383.

Zahn, R., Liu, A., Luehrs, T., Riek, R., von Schroetter, C., Garcia, F.L., Billeter, M., Calzolai, L., Wider, G. and Wüthrich, K. (2000). NMR solution structure of the human prion protein. *Proc. Natl. Acad. Sci. USA* 97, 145-150.

Appendices

1. A manuscript entitled “Amyloidogenesis in prion-infected cells.”

2. A paper entitled “Correlation of structural elements and infectivity of the HET-s prion” published in Nature (Ritter C, Maddelein M-L, Siemer AB, Luhrs T, Ernst M, Meier BH, Saupe SJ, and Riek R. 435, 844-848, 2005).

3. A meeting abstract entitled “The antemortem detection of prion proteins “ (NPRP Abstract 7-27-05) is attached as Appendix 3.

4. A list of personnel (not salaries) receiving pay from the research effort:

   David R. Schubert, Ph.D.
   Yuanbin Liu, Ph.D.
   Roland Riek, Ph.D.

The formation of bioactive amyloid species by prion proteins in vitro and in cells

Yuanbin Liu[1], Christiane Ritter[2], Roland Riek[2] and David Schubert[1]*

[1]Cellular Neurobiology Laboratory and [2]Structural Biology Laboratory, The Salk Institute for Biological Studies

*To whom correspondence should be addressed at

Cellular Neurobiology Laboratory

The Salk Institute for Biological Studies

10010 N. Torrey Pines Road

La Jolla, California 92037-1099

Phone: (858) 453-4100, x1528; Fax: (858) 535-9062

E-mail: schubert@salk.edu

Abstract:

Amyloid proteins are a group of proteins that can polymerize into cross β-sheeted amyloid species. We have found that enhancing cellular 3-(4,5-dimethylthiazol-2-yl)-2,5-diphenyltetrazolium bromide (MTT) formazan exocytosis is a common property of bioactive amyloid species formed from all of the amyloid proteins tested to date. In this report, we show that the infectious amyloid species of the prion protein HET-s of the filamentous fungus *Podospora anserina*, like other amyloidogenic proteins, also enhances MTT formazan exocytosis. More strikingly, cellular MTT formazan exocytosis revealed the formation of bioactive amyloid species in prion-infected mouse N2A neuroblastoma cells. These findings suggest that cellular MTT formazan exocytosis can be useful for studying the roles of bioactive amyloid species in prion infectivity and prion-induced neurodegeneration.

Key Words: Prion protein; amyloid; HET-s; MTT.

Introduction

The amyloidoses are a group of diseases in which normally soluble proteins polymerize into insoluble amyloid fibrils that then form amyloid deposits [1]. Although amyloid fibrils can be formed from proteins with different amino acid sequences, they all share the characteristic cross-β sheet structure in which the polypeptide backbones are oriented perpendicular to the long axis of the fibril [2]. Of about twenty known amyloid proteins, prion proteins are unique in that they are the only known infectious amyloidogenic proteins [1].

Our previous work with amyloid β protein (Aβ) in Alzheimer's disease and other amyloidogenic proteins (including human amylin, β-synuclein, artificially induced β-sheeted insulin and glucagons fibrils) has led to the development of a cell-based method for the detection of cross-β sheeted amyloid fibrils or subfibrillar species [3-9]. The method is based upon the observation that amyloidogenic proteins specifically and dramatically enhance the exocytosis of the intracellular vesicles that are involved in transporting the reduced tetrazolium dye 3-(4,5-dimethylthiazol-2-yl)-2,5-diphenyltetrazolium bromide (MTT formazan), with the formation of unique formazan crystals on the cell surface (Fig. 1A to C, compare formazan morphology between B and C). The exact form of the amyloidogenic proteins being detected by the MTT formazan phenomenon is not clear, but it is correlated with the formation of amyloid fibrils. The amyloid-binding dye Congo red and certain polysulfated glycosaminoglycans such as dextran sulfate can prevent or inhibit the ability of amyloidogenic proteins to induce MTT formazan exocytosis, suggesting that β-sheeted amyloid fibrils or subfibrillar structures are responsible for the phenomenon [4, 6, 8]. What is more striking with this phenomenon is its biological specificity. Aβ preparations that do not induce the unique MTT formazan crystals do not activate glia and are not toxic to primarily cultured rat hippocampal neurons [8], even though

microscopic examination revealed numerous amorphous aggregates. We therefore termed the species causing the unique MTT formazan crystals "bioactive amyloid species" [8, 9]. This cell-based method has proven useful in detecting bioactive amyloid species in a protein sample, in searching for anti-amyloid compounds, and in detecting the bioactive amyloid species in brains of animals and man [9].

Mammalian prion proteins [10, 11] as well as yeast prion proteins (Ure2p and Sup35p) and a fungal prion protein (HET-s) [12-14] are known to undergo self-seeded polymerization into amyloid-like fibrils. In the present report, we show that the cell-based MTT assay can be used to detect bioactive amyloid species formed by the prion protein HET-s of the filamentous fungus *Podospora anserina*, confirming that enhancing cellular MTT formazan exocytosis is a common biological property of amyloidogenic proteins, including prion proteins. More strikingly, mouse N2A neuroblastoma cells infected with the RML strain of mouse prion demonstrated spontaneous amyloidogenesis when studied with the cell-based assay. These results suggest that the cell-based MTT assay can be useful in the study of prion amyloidogenesis.

Materials and methods

Materials and cell lines. All amyloid peptides were obtained from Bachem California (Torrance, CA). All other reagents were from Sigma or Calbiochem. B12 cells are nerve-glial precursor cells from a collection of cells made from nitrosoethylurea-induced rat brain tumors [15]. Normal mouse N2A neuroblastoma cells were purchased from America Type Culture Collection (ATCC, Rockville, MD) and N2A cells infected with the RML strain of mouse prion (ScNB cells) were from NIH's Rocky Mountain Laboratories [16].

Photomicroscopy and quantitation of MTT formazan exocytosis. Cells growing on 35 mm dishes were incubated with MTT (0.5 mg/ml) for 30 min at 37°C, and then examined and photographed with a Nikon light microscope equipped with water immersible object lens and a digital color imaging system (Spot Insight, Diagnostic Instruments, Inc. MI). The needle-like crystals on the surface of the cells incubated with MTT, which are easily visible under a light microscope, represent exocytosed MTT formazan (Fig. 1 and [3]). The distinct MTT formazan crystals induced by amyloid peptides are best viewed with a 40x objective lens under phase. The percentage of cells exocytosing MTT formazan was determined by counting 300 cells in multiple fields using the presence of needle-like formazan crystals on cell surface as the indicator of MTT formazan exocytosis. A cell is counted as exocytosing MTT formazan as long as 3 or more needle-like formazan crystals are clearly visible.

Expression and purification of pHET constructs. The fungal prion protein HET-s was amplified and modified by polymerase chain reaction to contain a C-terminal His_6 tag and subsequently cloned into the NdeI and HindIII sites of the pET21a vector (Novagen) [17]. The E. coli strain BL21 (DE3) was transformed with the plasmid. 2 liters of LB medium were inoculated with an over-night culture and the bacteria were grown to an OD_{600} of 0.8-1.0 and induced with isopropyl-1-thio-β-D-galactopyranoside (1 mM) for 4 hours at 37°C. The pellet was washed in 50 mM Tris, pH 8.0, 150 mM NaCl, and then solubilized in 6 M guanidinium hydrochloride, 50 mM Tris pH 8.0, 150 mM NaCl. The protein constructs were purified by His_6 affinity chromatography using Ni-charged chelating agarose (Pharmacia). To refold the protein directly before use, it was incubated with 20 mM dithiothreitol for 20 min and subsequently applied to PD-10 desalting columns (Pharmacia) equilibrated with 50 mM Tris, pH 8.0, 150 mM

sodium chloride, 5 mM dithiothreitol. Recombinant HET-s forms amyloid fibrils spontaneously under these conditions.

Congo red birefringence. 10 μl of a protein fibril suspension was mixed with 10 μl 1% aqueous Congo red (pH 10) and was then placed on a glass slide. Birefringence was observed with a Nikon light microscope equipped with polarization filter.

Western blotting for protease-resistent prion protein (PrP-res or PrP^{SC}) accumulation in ScNB Cells. The immunoblot assay for PrP-res accumulation was performed as described previously [18]. Briefly, ScNB cells were lysed with detergents, cleared of debris with a low-speed centrifugation and treated with proteinase K to degrade protease-sensitive prion protein (PrP-sen or PrP^{C}). The PrP-res was pelleted by ultracentrifugation, solubilized in SDS/PAGE sample buffer, and run on 14% acrylamide precast Novex gels. Proteins were electroblotted onto Immobilon membranes (Millipore) and PrP was detected by using a polyclonal rabbit antiserum (R30) raised against a synthetic peptide corresponding to residues 89-103 of the mouse PrP amino acid sequence and a peroxidase-conjugated goat anti-rabbit secondary antibody. The blots were developed by using enhanced chemiluminescence reagents (Amersham).

Results and discussion

The fungal prion protein HET-s of *Podospora anserina* aggregates *in vitro* into infectious amyloid-like fibrils [17, 19]. We also found that HET-s monomers aggregate to form protein fibrils *in vitro* that show Congo red birefringence, an indication that the protein fibrils are amyloid fibrils (Fig. 1D). To test whether HET-s enhances cellular MTT formazan exocytosis like other amyloid proteins, B12 cells were incubated with HET-s fibrils overnight. As shown in

Fig. 1E and Table 1A, HET-s induced unique MTT formazan crystals which are morphologically identical to that induced by other amyloid proteins such as $A\beta_{1-42}$ (Fig. 1C). As a negative control, a HET-s protein sample denatured by trichloroacetic acid precipitation did not induce amyloid-like MTT formazan exocytosis (Fig. 1F and Table 1A). These results are an additional confirmation that enhancing cellular MTT formazan exocytosis is a common biological activity of amyloid proteins.

To test whether amyloidogenesis occurs in prion-infected cells, N2a neuroblastoma cells infected with the RML strain of mouse prion (ScNB cells, [16]) were examined for amyloid-induced cellular MTT formazan exocytosis directly without any other treatment. Fig. 2B (arrows) and Table 1B show that approximately 13% of the cells contained the characteristic amyloid-induced MTT formazan. N2A cells that were not infected with prion did not show this phenomenon (Fig. 2A). Treatment of the ScNB cells with 5 μM Congo red for 3 days, a known inhibitor of PrP-res accumulation [16], completely abolished amyloid-induced MTT formazan (Fig. 2C and Table 1B). Western blotting of PrP-res in N2a cells, ScNB cells and ScNB cells treated with 5 μM Congo red for 3 days shows that amyloid-induced MTT formazan exocytosis is strictly correlated with the presence of PrP-res (Fig. 2D). These results demonstrate that individual cells infected with prion can undergo amyloidogenesis and be detected by the cellular MTT formazan exocytosis assay.

In summary, the present study shows that amyloid species formed by prion proteins, like other amyloid proteins, enhance cellular MTT formazan exocytosis. Prion amyloidogenesis may play an important role in prion replication and in cellular damage caused by prion infection. Amyloid fibrils formed from recombinant prion proteins in vitro have been shown to be infectious [19-20], which supports a correlation between amyloid formation and infectivity.

Furthermore, a detailed structure-infectivity relationship study on HET-s suggests the HET-s amyloid is the infectious entity of the HET-s prion. Celluar MTT formazan exocytosis is a simple assay for detecting bioactive cross β-sheeted amyloid species, it therefore could be a useful tool for studying the relationship between amyloid formation and prion infectivity, replication and toxicity.

Acknowledgments We would like to thank Dr. Byron Caughey for providing and helping with the prion-infected cell lines, and Dr. Sven Saupe for providing the pHET-s expression vector. This work was supported by a grant from the Department of Defense (DAMD17-03-1-0285) to David Schubert, Yuanbin Liu and Roland Riek.

References

[1] J.D. Sipe, Amyloidosis, Ann. Rev. Biochem. 61 (1992) 947-975.

[2] G.G. Glenner, E.D. Eanes, H.A. Bladen, R.P. Linke, J.D. Termine, A comparison of native amyloid with synthetic protein fibrils, J. Histochem. Cytochem. 22 (1974) 1141-1158.

[3] Y. Liu, D. Peterson, H. Kimura, D. Schubert, The mechanism of cellular MTT reduction, J. Neurochem. 69 (1997) 581-593.

[4] Y. Liu, D. Schubert, Cytotoxic amyloid peptides inhibit cellular MTT reduction by enhancing MTT formazan exocytosis, J. Neurochem. 69 (1997) 2285-2293.

[5] Y. Liu, D. Peterson, D. Schubert D, Amyloid β peptide alters intracellular vesicle trafficking and cholesterol homeostasis, Proc. Natl. Acad. Sci. USA 95 (1998) 13266-13271.

[6] Y. Liu Y, D. Schubert, Steroid hormones block amyloid fibril-induced MTT formazan exocytosis: relationship to neurotoxicity, J. Neurochem. 71 (1998) 2322-2329.

[7] Y. Liu, Understanding the biological activity of amyloid proteins in vitro: from inhibited cellular MTT reduction to altered cellular cholesterol homeostasis, Prog. Neuro-Psychopharmacol. & Psychiat. 23 (1999) 377-395.

[8] Y. Liu, D. Piasecki, A cell-based method for the detection of nanomolar concentrations of bioactive amyloid, Anal. Biochem. 289 (2001) 130-136.

[9] Y. Liu, D. Dargusch, C. Banh, C.A. Miller, D. Schubert, Detecting bioactive amyloid β peptide species in Alzheimer's disease, J. Neurochem. 91 (2004) 648-656.

[10] S.B. Prusiner, M.P. McKinley, K.A. Bowman, D.C. Bolton, P.E. Bendheim, D.F. Groth, G.G. Glenner, Scrapie prions aggregate to form amyloid-like birefringent rods, Cell 35 (1983) 349-358.

[11] B.W. Caughey, A. Dong, K.S. Bhat, D. Ernst, S.F. Hayes, W.S. Caughey, Secondary structure analysis of the scrapie-associated protein PrP 27-30 in water by infrared spectroscopy, Biochemistry 30 (1991) 7672-7680.

[12] R.B. Wickner, K.L. Taylor, H.K. Edskes, M.L. Maddeleein, H. Moriyama, T. Roberts, Yeast prions act as genes composed of self-propagating protein amyloids, Adv. Prot. Chem. 57 (2001) 313-334.

[13] J.R. Glover, A.S. Kowal, E.C. Schirmer, M.M. Patino, J.J. Liu, S. Lindquist, Self-seeded fibers formed by Sup35, the protein determinant of [PSI+], a heritable prion-like factor of S. cerevisiae, Cell 89 (1997) 811-819.

[14] V. Coustou, C. Deleu, S. Saupe, J. Bégueret, The protein product of the *het-s* heterokaryon incompatibility gene of the fungus *Podospora anserina* behaves as a prion analog, Proc. Natl. Acad. Sci USA 94 (1997) 9773-9778.

[15] D. Schubert, S. Heinemann, W. Carlisle, H. Tarika, B. Kimes, J.H. Steinbach, W. Culp, B.L. Brandt, Clonal cell lines from the rat central nervous system, Nature 249 (1974) 224-227.

[16] B. Caughey B., R.E. Race, Potent inhibition of scrapie-associated PrP accumulation by Congo red, J. Neurochem. 59 (1992) 768-771.

[17] S. Dos Reis, B. Coulary-Salin, V. Forge, I. Lascu, J. Begueret, S.J. Saupe, The HET-s prion protein of the filamentous fungus Podospora anserina aggregates in vitro into amyloid-like fibrils, J Biol. Chem. 277 (2002) 5703-5706.

[18] W.S. Caughey, L.D. Raymond, M. Horiuchi, B. Caughey, Inhibition of protease-resistant prion protein formation by porphyrins and phthalocyanines, Proc. Natl. Acad. Sci. USA 95 (1998) 12117-12122.

[19] M.L. Maddelein, S. Dos Reis, S. Duvezin-Caubet, B. Coulary-Salin, S.J. Saupe, Amyloid

aggregates of the Het-s prion protein are infectious, Proc. Natl. Acad. Sci. 91 (2002) 648-656.

[20] G. Legname, I.V. Baskakov, H.O. Nguyen, D. Riesner, F.E. Cohen, S.J. DeArmond, S.B. Prusiner, Synthetic mammalian prions, Science 305 (2004) 673-676.

[21] C. Ritter, M.L. Maddelein, A.B. Siemer, T. Luhrs, M. Ernst, B.H. Meier, S.J. Saupe, R. Riek, Correlation of structural elements and infectivity of the HET-s prion, Nature 435 (2005) 844-848.

Table 1
Prion protein-induced MTT formazan exocytosis

Treatment	Percentage of cells shows amyloid-induced MTT formazan
A. Fungal prion protein HET-s	
Solvent control	0
1 μM $A\beta_{1-42}$	33 ± 5*
2 μM HET-s	21 ± 4*
2 μM denatured HET-s	0
B. Mammalian prion-infected N2a cells	
Normal N2a cells	0
ScNB cells	13 ± 5*
ScNB cells + 50 μM Congo red for 3 days	0 to 1

The effect of HET-s on cellular MTT formazan exocytosis by B12 cells was carried out as described in the legend of Fig. 1. The effect of prion infection on the cellular MTT formazan exocytosis of N2a cells was described in the legend of Fig. 2. All data are mean ± S.D. of four experiments. *: Significantly different from solvent control or normal N2a cells.

Figure Legends

Fig. 1. The fungal prion protein HET-s aggregates into amyloid fibrils in vitro and induces amyloid-like cellular MTT formazan exocytosis. B12 cells were treated as indicated, followed by 30 min or 3 hr of MTT (0.5 mg/ml) reduction. **(A)** Control, 30 min MTT reduction. **(B)** Control, 3 hr MTT reduction. Note the morphology of the naturally occurring MTT formazan. **(C)** 1 μM $A\beta_{1\text{-}42}$ overnight incubation followed by 30 min MTT reduction. The MTT formazan crystals are thicker, shorter and purple. **(D)** Congo red bifringence of HET-s amyloid fibrils. **(E)** HET-s was buffer exchanged from 6 M Guanidinium chloride to 50 mM Tris pH 8.0, 1 mM dithiothreitol. B12 cells were incubated with 2 μM HET-s overnight followed by 30 min MTT reduction. **(F)** The same as in **(E)** except HET-s in 6 M Guanidinium chloride was first precipitated with trichloroacetic acid.

Fig. 2. Detection of amyloidogenesis in prion-infected neuroblastoma cells with cellular MTT formazan exocytosis. Normal N2a cells **(A),** ScNB cells **(B)** and ScNB cells treated with 5 μM Congo red for 3 days **(C)** were incubated with MTT (0.5 mg/ml) for 60 min at 37°C and imaged under a light microscope. Arrows indicate cells with amyloid-induced MTT formazan crystals. **(D)** Western blotting of PrP-res: Line **1**, normal N2a cells; Line **2**, ScNB cells; line **3**, ScNB cells treated with 5 μM Congo red for 3 days.

Figure 1

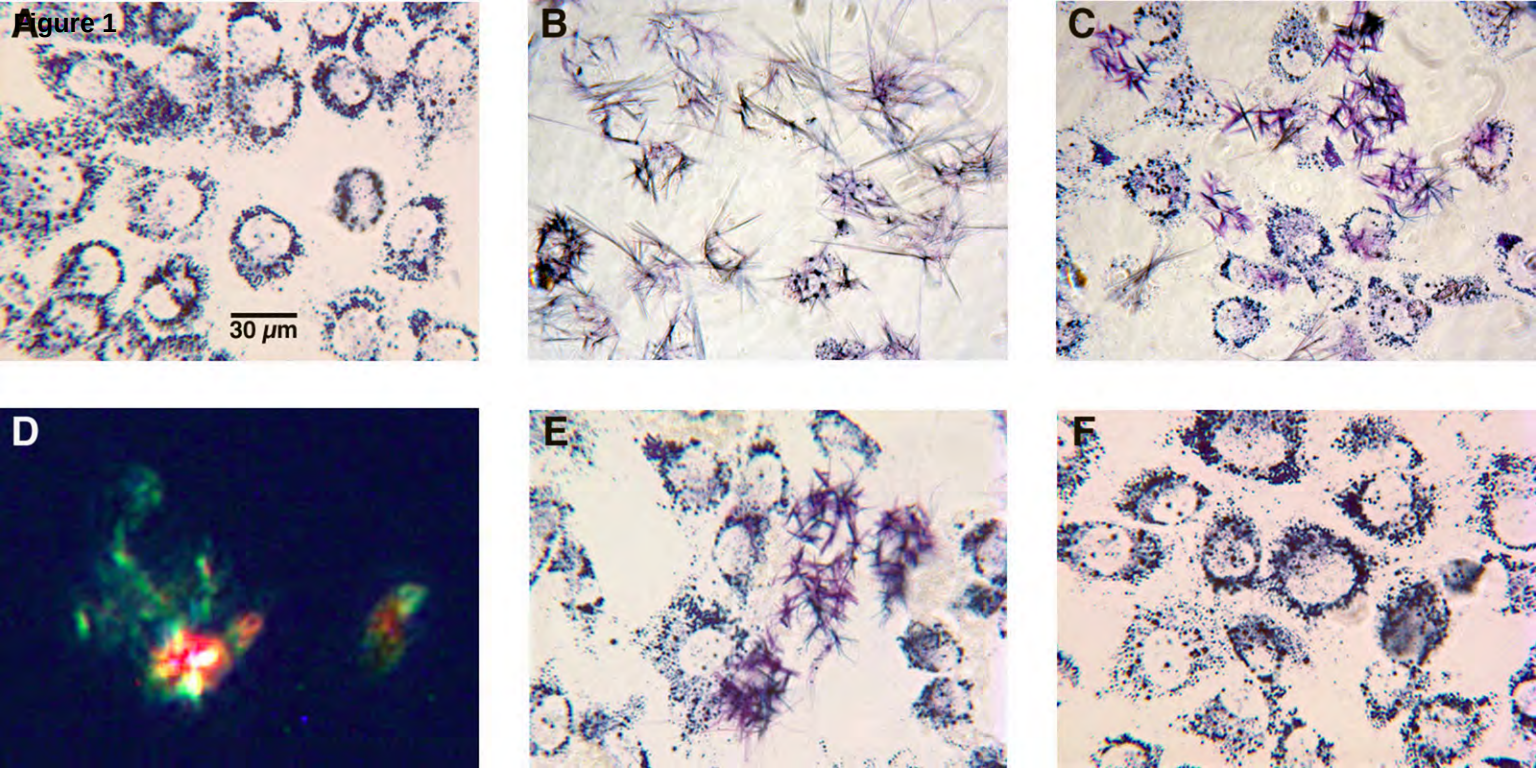

Figure 2

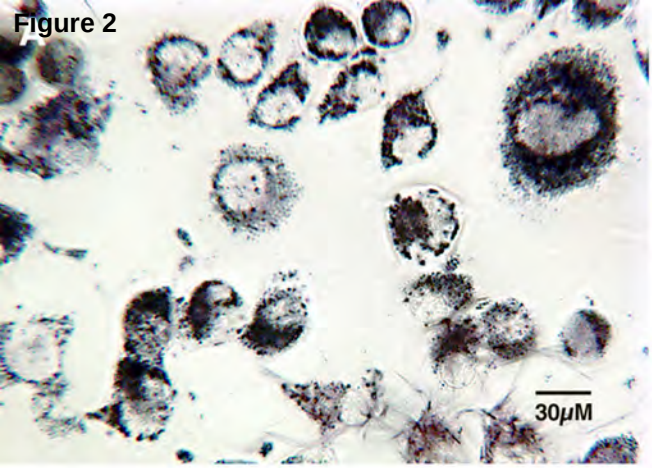

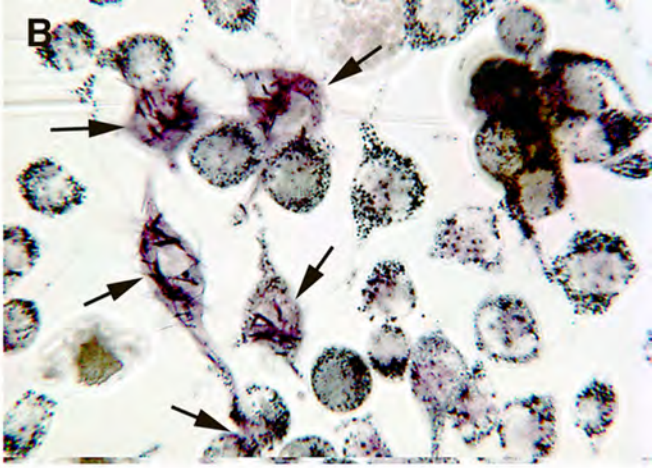

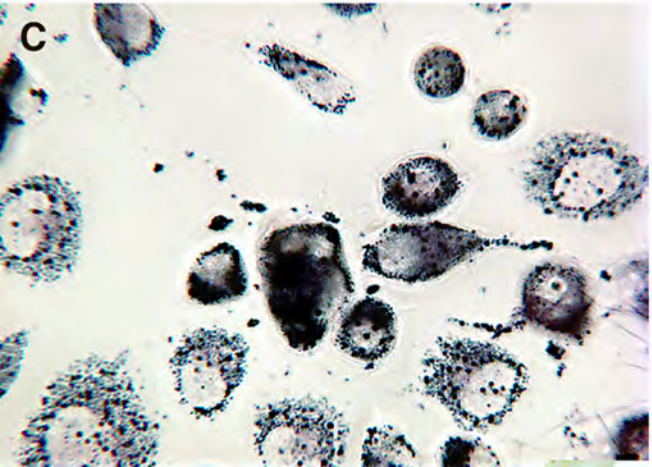

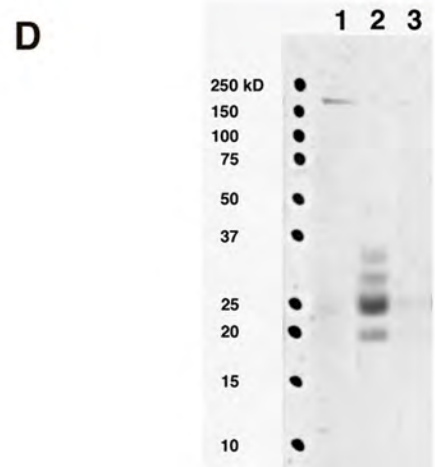

LETTERS

Correlation of structural elements and infectivity of the HET-s prion

Christiane Ritter[1]*, Marie-Lise Maddelein[2]*, Ansgar B. Siemer[3]*, Thorsten Lührs[1], Matthias Ernst[3], Beat H. Meier[3], Sven J. Saupe[2] & Roland Riek[1]

Prions are believed to be infectious, self-propagating polymers of otherwise soluble, host-encoded proteins[1,2]. This concept is now strongly supported by the recent findings that amyloid fibrils of recombinant prion proteins from yeast[3–5], *Podospora anserina*[6] and mammals[7] can induce prion phenotypes in the corresponding hosts. However, the structural basis of prion infectivity remains largely elusive because acquisition of atomic resolution structural properties of amyloid fibrils represents a largely unsolved technical challenge. HET-s, the prion protein of *P. anserina*, contains a carboxy-terminal prion domain comprising residues 218–289. Amyloid fibrils of HET-s(218–289) are necessary and sufficient for the induction and propagation of prion infectivity[6]. Here, we have used fluorescence studies, quenched hydrogen exchange NMR and solid-state NMR to determine the sequence-specific positions of amyloid fibril secondary structure elements of HET-s(218–289). This approach revealed four β-strands constituted by two pseudo-repeat sequences, each forming a β-strand-turn-β-strand motif. By using a structure-based mutagenesis approach, we show that this conformation is the functional and infectious entity of the HET-s prion. These results correlate distinct structural elements with prion infectivity.

The prion form of the protein HET-s is involved in a programmed cell death phenomenon termed heterokaryon incompatibility[8,9]. This reaction occurs in filamentous fungi when cells of incompatible genotype fuse and form a mixed cell. In *P. anserina*, two incompatible genotypes, called *het-s* and *het-S*, encode the proteins HET-s and HET-S, respectively. They are both 289 amino acids long and differ in only 13 residues[10]. However, only HET-s can form a prion[11]: *P. anserina* cells expressing the HET-s protein exist either in a prion state called [Het-s], or in a non-prion state called [Het-s*]. Infection of a [Het-s*] cell by a [Het-s] cell occurs by simple contact. The cell death reaction is triggered if a cell in the [Het-s] prion state fuses with a cell expressing HET-S. In contrast, a prion-free [Het-s*] cell can readily fuse with a cell expressing HET-S to form a viable mixed cell. Hence, the formation of the [Het-s] prion can easily be assayed by measuring its function in heterokaryon incompatibility. Both HET-s and the prion domain fragment HET-s(218–289) form amyloid fibrils *in vitro* that are infectious to [Het-s*] cells of *P. anserina*[6,12,13]. Transition to the prion state *in vivo* can also be detected by following the aggregation of a HET-s–green fluorescent protein (GFP) fusion protein[14,15].

To elucidate the fold of the amyloid fibrils of HET-s(218–289), we first identified the sequence-specific positions of regular secondary structural elements using an improved technique of quenched hydrogen exchange measured by solution NMR[16] (see Methods). This technique allows the identification of solvent-protected backbone amide protons involved in hydrogen bonds. The [^{15}N,^{1}H] correlation NMR spectrum (Fig. 1a) contained one assigned cross-peak for each backbone amide of HET-s(218–289), with the exception of 289, enabling a residue-specific determination of the hydrogen exchange rates. Upon exchange in D_2O buffer for 6 weeks, the intensity of about 45% of the resonances was significantly reduced or absent from the spectrum (Fig. 1b). This suggested that the corresponding amides have undergone exchange with solvent deuterons, which are not visible in this experiment.

The hydrogen exchange was followed over a total period of 3 months. All residues displayed a monoexponential decay (Supplementary Fig. S1), indicating that the structure of the fibrils was well defined and homogeneous. The summarized hydrogen exchange data (Fig. 1e) show that owing to exchange rates faster than $5\,h^{-1}$, the eight amino-terminal residues, the five carboxy-terminal residues and residues 247–261 are only weakly or not protected and may therefore be conformationally disordered. Four segments were observed that displayed slow exchange rates of $10^{-2}\,h^{-1}$ to $10^{-5}\,h^{-1}$ and were thus considered to be involved in hydrogen bonds. They comprise residues 226–234, 236–246, 262–270 and 272–282. Similarly slow exchange rates have been observed for Aβ (1–42) fibrils[17] and reflect the extraordinary stability and compactness amyloid fibrils can achieve. Because circular dichroism experiments have established that the HET-s(218–289) fibrils contain mainly β-sheet secondary structure[13], it is likely that the four protected segments represent four distinct β-strands. Hydrogen exchange data were also accumulated for amyloid fibrils of the full-length HET-s protein. The protection pattern of the peptide segment 218–288 in HET-s was essentially identical to that of HET-s(218–289) (Supplementary Fig. S2). This suggests that the prion domain acts as an independent folding unit.

To determine which residues are actually involved in β-sheet secondary structure, high-resolution solid-state NMR spectra of the HET-s(218–289) fibrils were recorded. The ^{13}C–^{13}C homonuclear DREAM[18] correlation spectrum of uniformly ^{15}N and ^{13}C isotope-labelled amyloid fibrils is shown in Fig. 1c, d. The resonance lines are strikingly narrow (down to 0.2 p.p.m.) and are comparable to those of micro-crystalline proteins, indicating a highly ordered atomic structure for part of the fibrils. Sequence-specific chemical shift assignment could be obtained for residues 226–248 and 262–282 (with the exception of 274). The missing resonances of the remaining residues are probably a consequence of dynamical or structural heterogeneity[19]. Deviations of the combined ^{13}Cα/^{13}Cβ chemical shifts from random coil values were used to identify the type of secondary structure present in HET-s(218–289) fibrils. Negative deviations (Fig. 1f) indicated β-sheet secondary structure[20] for

[1]The Salk Institute, 10010 North Torrey Pines Road, La Jolla, California 92037, USA. [2]Laboratoire de Génétique Moléculaire des Champignons, Institut de Biochimie et de Génétique Cellulaires, Unité Mixte de Recherche 5095, Centre national de la Recherche Scientifique Université de Bordeaux 2, 33077 Bordeaux Cedex, France. [3]ETH Zurich, Physical Chemistry, ETH Honggerberg, 8093 Zurich, Switzerland.
*These authors contributed equally to this work.

residues 226–234, 237–244, 262–271 and 273–282. Exceptions were observed at residues 229 and 265 (see below) and, to a lesser degree, at 277. Chemical shift assignment by solid-state NMR was achieved for all residues that showed slow hydrogen exchange (Fig. 1e). The striking correlation between the exchange data (Fig. 1e) and the chemical shift data (Fig. 1f) allowed for the confident establishment of secondary structure in the HET-s(218–289) amyloid fibrils: four β-strands comprising residues ~226–234 (β1), ~237–245 (β2), ~262–270 (β3) and ~273–282 (β4) are connected by two short loops between β1 and β2, and β3 and β4, respectively, and by an unstructured, 15-residue-long segment between β2 and β3.

To determine the topology of β-strands in HET-s(218–289) fibrils, we made use of the architecture of β-sheets, in which the side chains of the even-numbered residues face in one direction, and those of the odd-numbered residues face in the opposite direction. Therefore, single cysteine residues were introduced at the odd- and

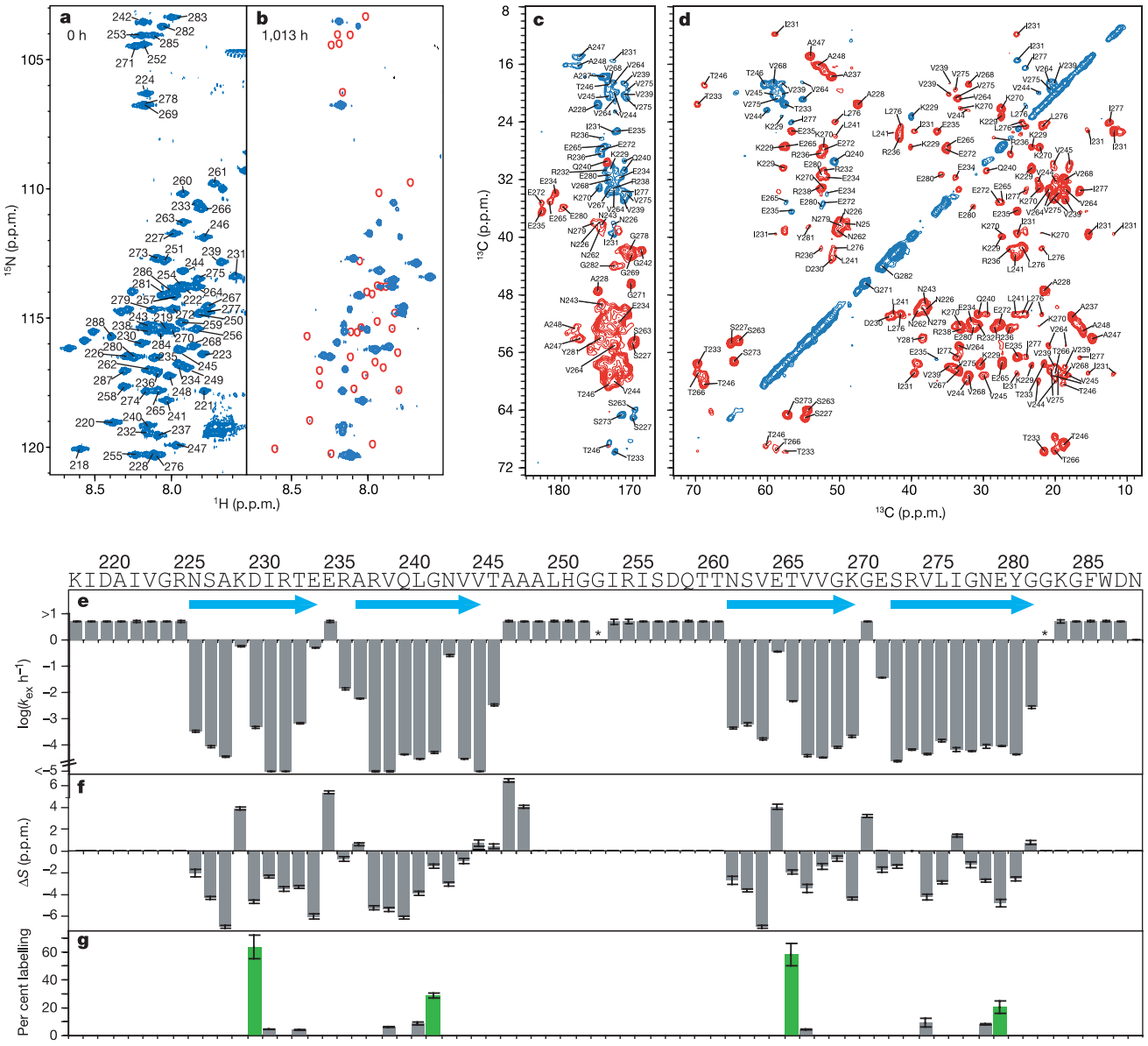

Figure 1 | Sequence-specific determination of regular secondary structure and its topology in HET-s(218-289) fibrils. a, **b**, Fast HMQC spectra of homogenously ^{15}N-labelled HET-s(218–289) in d_6-DMSO containing 0.1% d_1-TFA, corresponding to fully protonated (**a**) and partially hydrogen exchanged (**b**) amyloid fibrils. Sequence-specific chemical shift assignments are labelled. Red lines encircle cross-peaks that show a virtually complete loss of intensity after $t_{ex} = 6$ weeks. **c**, **d**, Homonuclear ^{13}C–^{13}C DREAM correlation spectra of ^{13}C,^{15}N-labelled HET-s(218–289) fibrils. The carbonyl region of the DREAM spectra (**c**) was recorded at 40 kHz MAS. Positive contours (blue) were taken from a spectrum recorded with an up–down tangential DREAM sweep; negative contours (red) were taken from a similar spectrum but with a down–up sweep. Contour levels start at approximately 2.5 times root mean square (r.m.s.) noise level and increase by a factor of 1.4. Representative traces through the two-dimensional spectra are given in Supplementary Fig. S5. The aliphatic region of a DREAM spectrum (**d**) was recorded at 25 kHz MAS. Sequence-specific chemical shift assignments are labelled. **e**, Plots of the observed quenched hydrogen exchange rates k_{ex} h^{-1}. The measurable upper limit was 5 h^{-1}. Error bars indicate deviations from a monoexponential fit. Asterisks denote residues that could not be analysed, blue arrows the location of β-strands. **f**, Plot of $\Delta S = \Delta(\delta(^{13}C\alpha)) - \Delta(\delta(^{13}C\beta))$. $\Delta(\delta(^{13}C\alpha))$ and $\Delta(\delta(^{13}C\beta))$ are the difference between experimental ^{13}Cα and ^{13}Cβ chemical shifts and the corresponding 'random coil' chemical shifts. The line-width- and peak-overlap-dependent accuracy for each value is indicated. **g**, Solvent accessibility of single cysteine mutants. The fluorescence intensity of Alexa Fluor 488 crosslinked to the cysteine side chains is given relative to a positive control (see Methods) at the position at which the cysteine was introduced. Even-numbered positions are shown in green. Error bars indicate s.d. of at least three independent experiments.

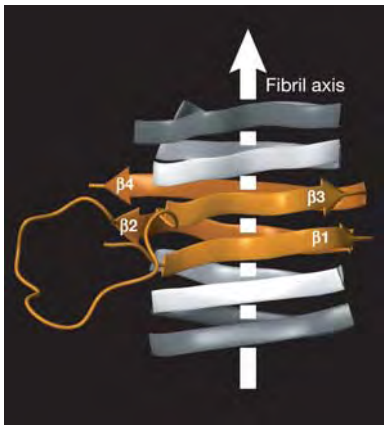

Figure 2 | The proposed fold of the infectious conformation of HET-s(218–289) amyloid fibrils. The extent and position in primary sequence of the β-strands is obtained from NMR data; the relative spatial position of the β-strands is modelled, taking into account the hydrophobicity of the residues, the high sequence identity between β-strands 1 and 3 and 2 and 4, and solvent accessibility data. There are, however no direct inter-strand distance constraints. A model is shown as an orange ribbon diagram, flanked by neighbouring molecules indicated in white. β-strands are indicated by arrows, non-regular secondary structures by spine curves through the Cα atoms of the corresponding residues, and the fibril axis by a white arrow. The β-strands are labelled.

even-numbered sides of each β-strand. Solvent accessibility was then probed by chemical crosslinking[21] with a fluorescent dye using Alexa Fluor 488 C_5 maleimide. The extent of solvent accessibility of 11 Cys residues is shown in Fig. 1g. The even-numbered residues of each strand displayed high crosslinking rates, whereas all odd numbered sides remained unlabelled. This indicated that all β-sheets have one solvent-accessible side.

The acquired structural data (Fig. 1) allowed us to propose a likely fold for the HET-s(218–289) fibrils (Fig. 2): the core of the fibrils consists of two β-strand-turn-β-strand motifs comprising β1 and β2 and β3 and β4, respectively, which are interconnected by a long loop formed by residues 246–261. The two segments interact through hydrogen bonding between β1 and β3, and β2 and β4, respectively, forming two layers of parallel β-sheets. The β-sheets continue along the fibril axis through intermolecular hydrogen bonding between neighbouring molecules (Fig. 2). The proposed fold is consistent with the NMR data, the observed pattern of solvent accessibility, the distribution of polar and hydrophobic residues on each strand, and the short loops between β1 and β2, and β3 and β4, respectively. It also takes into account the remarkable sequence identity of 28% between the segments β1–β2 and β3–β4, which suggests a repetitive arrangement (Supplementary Fig. S3). The only charged residues facing towards the inside of the fibril are K229 in β1 and E265 in β3, which are located in adjacent positions in the proposed fold, and therefore able to compensate their opposite charges. The reduced protection against hydrogen exchange of these residues as well as their non-beta solid-state chemical shifts (Fig. 1e, f) indicate a structural disturbance of the β-sheets at the positions of the proposed salt bridge.

In order to correlate the proposed fold of the HET-s(218–289) fibrils with [Het-s] function and infectivity, a mutational approach was used. Because the fold is based on β-sheet secondary structure, we introduced proline residues, which are known to act as local β-strand breakers. A series of 13 mutants was generated with a single proline substitution approximately every five residues in the 218–289 region of full-length HET-s (Fig. 3a). A number of short deletion mutants affecting the central loop and the β-strand segments were also generated (Fig. 3b). *P. anserina* transformants expressing the

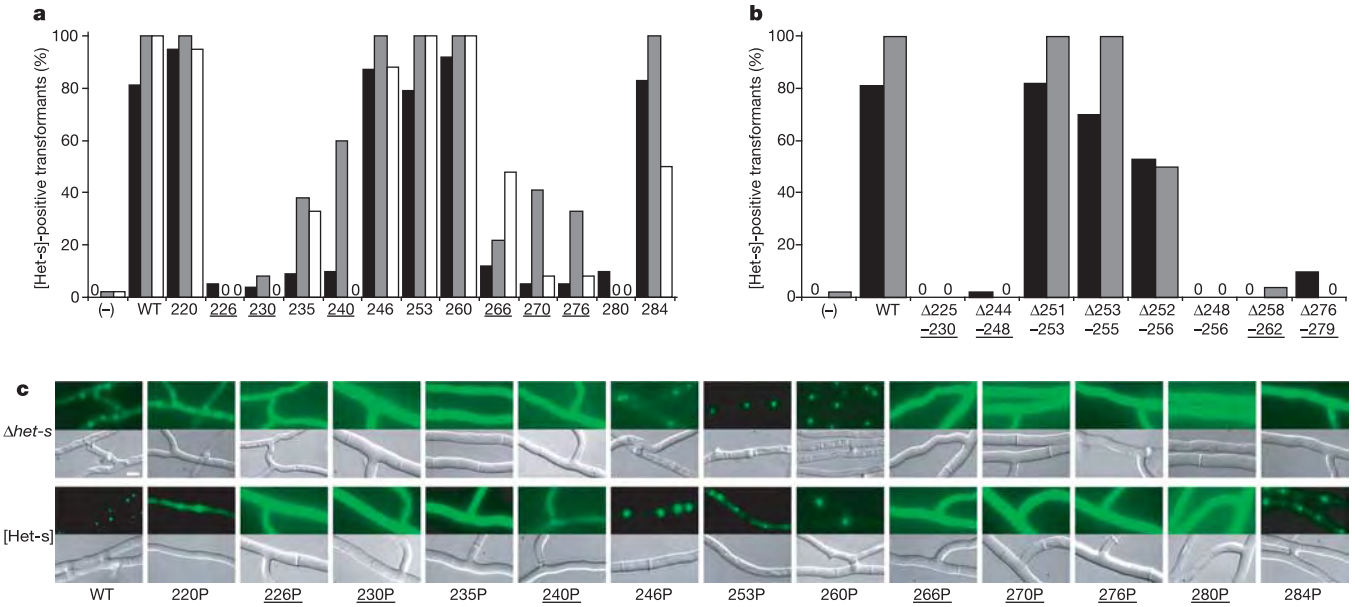

Figure 3 | *In vivo* prion formation of HET-s proline and deletion mutants. **a**, Proline mutants were introduced into a *Δhet-s P. anserina* strain and the transformants prion-infected by confrontation with a [Het-s] colony. Given are the percentage of transformants producing a cell death reaction when confronted with a *het-S* tester colony (black columns), and the percentage of transformants displaying [Het-s] infectivity immediately after infection (grey columns) and after a 3-day subculture (white columns). The minus sign indicates vector alone, and WT indicates wild-type HET-s; mutants are labelled by the position of the proline. Zero indicates that all transformants were negative. **b**, Deletion mutants of HET-s were expressed in a *Δhet-s* strain and the transformants prion-infected as above. Colour code as in **a**. **c**, *In vivo* aggregation of HET-s–GFP fusion proteins with proline substitutions. Wild-type and mutant HET-s–GFP fusion proteins were expressed either in a *Δhet-s* knockout strain or a wild-type prion-infected [Het-s] strain. Transformants of the *Δhet-s* background were prion-infected by contact with a wild-type [Het-s] strain before microscopic observation. Scale bar, 4 μm. Mutants located in β-strand elements are underlined. A complete data set with the numbers of individual transformants tested is given in Supplementary Table 1.

mutant proteins were prion-infected by contact with a wild-type [Het-s] colony. The presence of [Het-s] prions in these transformants was then assayed by monitoring their ability to produce a cell death reaction when fused to a HET-S-expressing colony, and to infect a prion-free [Het-s*] colony. [Het-s] infectivity was assayed immediately after contact of the transformants with the wild-type [Het-s] donor and again after a 3-day subculture (Fig. 3a; see also Supplementary Table 1). In order to monitor the formation of HET-s aggregates *in vivo*, the same mutations were introduced in a HET-s–GFP fusion protein. The mutant fusion proteins were over-expressed both in *P. anserina Δhet-s* knockout strains and in a [Het-s] strain in order to determine whether co-expression with endogenous wild-type prions would lead to aggregation of the mutant fusion proteins (Fig. 3c).

In striking correlation with the structural data, proline substitutions located in the β-strand regions strongly affected [Het-s] function, infectivity (Fig. 3a) and HET-s–GFP foci formation (Fig. 3c). In contrast, proline substitutions in the N- or C-terminal flexible tails or the central loop did not affect [Het-s] activity, infectivity, or HET-s–GFP foci formation. Similarly, the deletions Δ225–230, Δ244–248, Δ258–262 and Δ276–279, which affected the β-strand elements, abolished [Het-s] infectivity. Short deletions of no more than three amino acids in the central loop did not affect [Het-s], but a larger deletion, Δ248–256, led to loss of [Het-s] function and infectivity. This indicates that a minimal length in the central loop might be required.

For some mutations in β-strand positions, [Het-s] prion infectivity could be detected transiently, but was lost upon subculturing (for instance, HET-s 240P, Fig. 3a). Concomitantly, GFP foci formation of HET-s 240P was detected only when the mutant protein was co-expressed with wild-type [Het-s] prions (Fig. 3b). This suggests that these mutant proteins retained a certain ability to form [Het-s] prions, but that they are mitotically very unstable. In addition, a number of proline substitutions in β-strand regions and in the short connecting loop did not lead to a total loss of [Het-s] function or infectivity, indicating that they interfered only partially with amyloid formation. Indeed, recombinant HET-s 226P and 266P retained a residual ability to form amyloid fibrils *in vitro* and to infect prion-free [Het-s*] colonies when introduced biolistically (Supplementary Fig. S4 and Supplementary Table 2). Interestingly, HET-s 246P retained [Het-s] activity. Residue 246 is still involved in hydrogen bonding, but has an α-helical rather than a β-sheet chemical shift. This suggests that it is specifically the β-sheet secondary structure that is required for HET-s function and infectivity.

Taken together, the local disruption of any of the four β-strands reduced or even abolished the formation and function of the [Het-s] prion, whereas the central loop only required a certain minimal length to sustain prion formation.

Our data correlate strongly the amyloid conformation with infectivity. Hence, the proposed fold of the HET-s(218–289) fibrils shown in Fig. 2 represents an infectious protein conformation. Because the [Het-s] prion has a natural function in heterokaryon incompatibility, it seems plausible that this infectious conformation was evolutionarily optimized for amyloid fibril formation. This view is supported by the extraordinarily well-ordered structure as manifested in the narrow line width observed in the solid-state NMR spectra, and the monoexponential hydrogen exchange rates. In contrast, other amyloid fibrils associated with misfolding diseases appear to be structurally more heterogeneous[22–25]. Furthermore, the dimer-like double β-strand-turn-β-strand motif formed by the pseudo-repeats β1–β2 and β3–β4 may have evolved to optimise the polymerization: in the case of a single β-strand-turn-β-strand motif, the initial step of fibril growth requires the diffusion-dependant formation of an oligomeric nucleus[26]. The covalent nature of the pseudo-repeats is therefore likely to promote this nucleation event by reducing its diffusion dependency.

It is generally believed that most prions will share β-sheet-rich amyloid fibrils as a common structural feature. Here, we have now shown that a β-sheet structure is indeed the infectious prion conformation of HET-s. This link between structure and infectivity constitutes a significant step towards the elucidation of the mechanism of prion formation and propagation.

METHODS

Mutagenesis. All site-directed mutants were generated with the Quick-change kit (Stratagene) using the pCB1004-het-s, pGPD-het-s–GFP[14] and the pET-21a-het-s vectors as template[12].

Preparation of stable-isotope-labelled HET-s(218–289) fibrils. Stable-isotope-labelled HET-s(218–289) was expressed as described for other HET-s constructs[13]. The bacterial pellet was solubilized in 50 mM TRIS pH 8.0 and 150 mM sodium chloride (TCl) containing 6 M guanidinium hydrochloride. The supernatant was centrifuged for 30 min at 18,000*g*. The protein was purified from the supernatant by His_6-affinity chromatography and concentrated to approximately 0.5–1 mM. Fast buffer exchange to TCl buffer yielded monomeric HET-s(218–289), which started to aggregate immediately into amyloid fibrils.

Hydrogen exchange. ^{15}N-labelled HET-s(218–289) was used. To reduce the size of large clumps of fibrils, a suspension of the fibrils in liquid nitrogen was bruised with a mortar. To start the hydrogen exchange, the fibrils were sedimented at 3,600*g* for 10 min, washed with 50 mM TRIS pH 8.0^{read} containing 150 mM sodium chloride, 5 mM dithiothreitol and D_2O as the solvent, and re-suspended in the same buffer. At suitable intervals, aliquots were sedimented at 24,000*g* for 2 min, washed with D_2O and frozen in liquid nitrogen to quench hydrogen exchange. For the NMR analysis, the fibrils were dissociated in perdeuterated dimethylsulphoxide (d_6-DMSO) containing 0.1% deuterated trifluoroacetic acid (d_1-TFA). The amount of residual D_2O was about 3%. Immediately after dissolving the fibrils, a series of 80 two-dimensional [^{15}N,^{1}H] correlation spectra were measured for 8 h. To distinguish residues that display fast exchange in the fibrils and residues that have high intrinsic exchange rates in DMSO, which would both result in absent peaks in the [^{15}N,^{1}H] correlation spectrum[17], a second series of 80 two-dimensional spectra were measured upon addition of 3% H_2O. Using this control measurement, residues 253 and 283 were excluded form the analysis. With the exception of the amide group of N289, a complete sequence-specific assignment of the backbone H^N/N cross-peaks was obtained using the triple-resonance experiments HNCA[27] and HNCA(CO)NH[28] applied to ^{13}C,^{15}N-labelled HET-s(218–289). The data were analysed using the programs PROSA[29] and CARA (http://www.nmr.ch), and a specially written Visual basic program in combination with Microsoft Excel[17].

Solid-state NMR. The HET-s(218–289) fibrils were washed in H_2O and centrifuged into MAS rotors sealed with two-component epoxy adhesive to prevent dehydration. Solid-state NMR spectra were recorded on a Bruker AV600 spectrometer at a static field of 14.09 T. A 2.5-mm Chemagnetics probe was used for the experiments at 25 kHz MAS and a 1.8-mm probe constructed by A. Samoson[30] for the experiments at 40 kHz MAS. The sample temperature was kept at 5–15 °C. For the ^{13}C–^{13}C correlation spectra recorded using the DREAM scheme[18], the contact time of the initial adiabatic cross-polarization was 1 ms and the RF-field strengths were 70 kHz and 90 kHz for ^{13}C and ^{1}H at 25 kHz MAS, and 90 kHz and 130 kHz for ^{13}C and ^{1}H at 40 kHz MAS, respectively. Continuous wave decoupling was applied during the DREAM mixing step and XiX decoupling during t_1 and t_2, both with an RF-field amplitude of 150 kHz. The measurement time was 33 h and 55 h for the experiments at 25 kHz and 40 kHz MAS, respectively. These spectra we used for the identification of spin systems and the ^{13}C side-chain assignment. For the backbone assignment we recorded the following heteronuclear two-dimensional correlation spectra: NCA, NCO, N(CA)CO, N(CA)CB and N(CO)CA. The assignment was done using the CARA program (http://www.nmr.ch) and confirmed via a CA–CA correlation spectrum.

Side-chain solvent accessibility studies. Proteins were purified as described above. Fibrils were reduced with 20 mM dithiothreitol before the final buffer exchange, and re-natured under nitrogen. To label solvent-accessible Cys residues by chemical crosslinking, 85 μM fibrils were incubated with a 2.5-fold molar excess of Alexa Fluor 488 C_5 maleimide (Molecular Probes) for 20 min at room temperature. The fibrils were washed extensively with TCl buffer and solubilized with 8 M spectroscopically pure guanidine hydrochloride. For fluorometry, the samples were diluted at least 70-fold into TCl buffer. The Alexa Fluor 488 fluorescence (excitation 493 nm, emission 516 nm) was measured relative to the fluorescence of a single Trp residue in HET-s(218–289) (excitation 295 nm, emission 353 nm). To determine the maximum labelling efficiency, the mutant HET-s(218–289) D288C was used, which is located in the presumably solvent accessible C-terminal region showing fast

hydrogen exchange. Wild-type HET-s(218–389) fibrils were labelled to $1.9 \pm 0.1\%$.

***In vivo* analysis of HET-s mutants.** *het-s* mutant alleles were introduced in the *Δhet-s* and wild-type *het-s* recipient strains[10]. [Het-s] incompatibility function, [Het-s] infectivity and HET-s–GFP foci formation were analysed as described previously[15]. After their initial contact with the [Het-s] prion donor, the transformants were either subcultured for 3 days or directly confronted with the [Het-s*] recipient in order to be able to detect transient expression of the [Het-s] state. Under the tested conditions, spontaneous emergence of [Het-s] in [Het-s*] colonies is in the range of 2%.

Received 4 March; accepted 12 May 2005.

1. Alper, T., Cramp, W. A., Haig, D. A. & Clarke, M. C. Does the agent of scrapie replicate without nucleic acid? *Nature* **214,** 764–766 (1967).
2. Prusiner, S. B. Novel proteinaceous infectious particles cause scrapie. *Science* **216,** 136–144 (1982).
3. Sparrer, H. E., Santoso, A., Szoka, F. C. Jr & Weissman, J. S. Evidence for the prion hypothesis: induction of the yeast [PSI+] factor by *in vitro*-converted Sup35 protein. *Science* **289,** 595–599 (2000).
4. King, C. Y. & Diaz-Avalos, R. Protein-only transmission of three yeast prion strains. *Nature* **428,** 319–323 (2004).
5. Tanaka, M., Chien, P., Naber, N., Cooke, R. & Weissman, J. S. Conformational variations in an infectious protein determine prion strain differences. *Nature* **428,** 323–328 (2004).
6. Maddelein, M. L., Dos Reis, S., Duvezin-Caubet, S., Coulary-Salin, B. & Saupe, S. J. Amyloid aggregates of the HET-s prion protein are infectious. *Proc. Natl Acad. Sci. USA* **99,** 7402–7407 (2002).
7. Legname, G. *et al.* Synthetic mammalian prions. *Science* **305,** 673–676 (2004).
8. Glass, N. L. & Kaneko, I. Fatal attraction: nonself recognition and heterokaryon incompatibility in filamentous fungi. *Eukaryot. Cell* **2,** 1–8 (2003).
9. Saupe, S. J. Molecular genetics of heterokaryon incompatibility in filamentous ascomycetes. *Microbiol. Mol. Biol. Rev.* **64,** 489–502 (2000).
10. Turcq, B., Deleu, C., Denayrolles, M. & Begueret, J. Two allelic genes responsible for vegetative incompatibility in the fungus *Podospora anserina* are not essential for cell viability. *Mol. Gen. Genet.* **228,** 265–269 (1991).
11. Coustou, V., Deleu, C., Saupe, S. & Begueret, J. The protein product of the het-s heterokaryon incompatibility gene of the fungus *Podospora anserina* behaves as a prion analog. *Proc. Natl Acad. Sci. USA* **94,** 9773–9778 (1997).
12. Dos Reis, S. *et al.* The HET-s prion protein of the filamentous fungus *Podospora anserina* aggregates *in vitro* into amyloid-like fibrils. *J. Biol. Chem.* **277,** 5703–5706 (2002).
13. Balguerie, A. *et al.* Domain organization and structure-function relationship of the HET-s prion protein of *Podospora anserina*. *EMBO J.* **22,** 2071–2081 (2003).
14. Coustou-Linares, V., Maddelein, M. L., Begueret, J. & Saupe, S. J. *In vivo* aggregation of the HET-s prion protein of the fungus *Podospora anserina*. *Mol. Microbiol.* **42,** 1325–1335 (2001).
15. Balguerie, A. *et al.* The sequences appended to the amyloid core region of the HET-s prion protein determine higher-order aggregate organization *in vivo*. *J. Cell Sci.* **117,** 2599–2610 (2004).
16. Hoshino, M. *et al.* Mapping the core of the β2-microglobulin amyloid fibril by H/D exchange. *Nature Struct. Biol.* **9,** 332–336 (2002).
17. Lührs, T. *et al.* The 3D structure of Alzheimer's Aβ(1–42) fibrils. *Nature* (submitted).
18. Verel, R., Ernst, M. & Meier, B. H. Adiabatic dipolar recoupling in solid-state NMR: The DREAM scheme. *J. Magn. Reson.* **150,** 81–99 (2001).
19. Siemer, A. B., Ritter, C., Ernst, M., Riek, R. & Meier, B. H. High-resolution solid-state NMR of the prion protein HET-s in its amyloid conformation. *Angew. Chem. Int. Edn Engl.* **44,** 2441–2444 (2005).
20. Wishart, D. S. & Sykes, B. D. The ^{13}C chemical-shift index: a simple method for the identification of protein secondary structure using ^{13}C chemical-shift data. *J. Biomol. NMR* **4,** 171–180 (1994).
21. Javitch, J. A., Shi, L. & Liapakis, G. Use of the substituted cysteine accessibility method to study the structure and function of G protein-coupled receptors. *Methods Enzymol.* **343,** 137–156 (2002).
22. Tycko, R. Progress towards a molecular-level structural understanding of amyloid fibrils. *Curr. Opin. Struct. Biol.* **14,** 96–103 (2004).
23. Petkova, A. T. *et al.* Self-propagating, molecular-level polymorphism in Alzheimer's β-amyloid fibrils. *Science* **307,** 262–265 (2005).
24. Laws, D. D. *et al.* Solid-state NMR studies of the secondary structure of a mutant prion protein fragment of 55 residues that induces neurodegeneration. *Proc. Natl Acad. Sci. USA* **98,** 11686–11690 (2001).
25. Yamaguchi, K. *et al.* Core and heterogeneity of β2-microglobulin amyloid fibrils as revealed by H/D exchange. *J. Mol. Biol.* **338,** 559–571 (2004).
26. Harper, J. D. & Lansbury, P. T. Jr Models of amyloid seeding in Alzheimer's disease and scrapie: mechanistic truths and physiological consequences of the time-dependent solubility of amyloid proteins. *Annu. Rev. Biochem.* **66,** 385–407 (1997).
27. Grzesiek, S. *et al.* ^{1}H, ^{13}C, and ^{15}N NMR backbone assignments and secondary structure of human interferon-γ. *Biochemistry* **31,** 8180–8190 (1992).
28. Bracken, C., Palmer, A. G. III & Cavanagh, J. (H)N(COCA)NH and HN(COCA)NH experiments for ^{1}H–^{15}N backbone assignments in $^{13}C/^{15}N$-labeled proteins. *J. Biomol. NMR* **9,** 94–100 (1997).
29. Guntert, P., Dotsch, V., Wider, G. & Wuthrich, K. Processing of multidimensional NMR data with the new software Prosa. *J. Biomol. NMR* **2,** 619–629 (1992).
30. Samoson, A., Tuherm, T. & Past, J. Rotation sweep NMR. *Chem. Phys. Lett.* **365,** 292–299 (2002).

Supplementary Information is linked to the online version of the paper at www.nature.com/nature.

Acknowledgements R.R. is a Pew scholar. This research was supported in part by grants from the National Institute of Health, the US Army, the ETH Zurich, the Swiss National Science Foundation, the CNRS and the French Ministry of Research.

Author Information Reprints and permissions information is available at npg.nature.com/reprintsandpermissions. The authors declare no competing financial interests. Correspondence and requests for materials should be addressed to R.R. (riek@salk.edu).

NPRP Abstract 7-27-05

TITLE: THE ANTEMORTEM DETECTION OF PRION PROTEINS

CO-PRINCIPAL INVESTIGATORS:
David R. Schubert, Ph.D.
Yuanbin Liu, Ph.D.
Roland Riek, Ph.D.

ABSTRACT:

The aim of our research is to develop an antemortem test for prion diseases based on a non-immunological, cell-based biological assay for the detection of PrP amyloid species. In addition, we focus on elucidating the infectious entity of prions and the molecular mechanism of generating prion infectivity. Blood from animals with prion disease contain low levels of prion infectivity, which primarily resides in the “buffy coat” fraction that contains lymphocytes and mononuclear cells. We believe that detecting individual infected white blood cells (WBCs) may increase the detection sensitivity by over 100-fold when compared with a method using pooled cells. We initially showed that a tetrazolium dye called MTT is able to detect biologically active amyloidogenic proteins, including prion proteins in single cells. This assay worked fine on cultured nerve and glial cells, but failed to be useful for the detection of prion infected lymphoid cells because of the high background in these cells. Since this assay ultimately turned out not to work, we have developed an alternative method that combines WBC isolation and cell blotting of PrP^{sc} to detect individual cells that contain PrP^{sc}. A sensitivity study shows that as low as 10 to 50 prion-infected cells can be detected, suggesting that it may have the potential to be used for the antemortem detection of prion infection in blood. In the second part of the project we initiated structural studies on HET-s, the prion protein of the fungus, P. anserina. The structural basis of prion infectivity and the origin and mechanism of infectivity has been elusive because acquisition of atomic resolution structural properties of amyloid fibrils represents an unsolved technical challenge. The C-terminal prion domain of HET-s comprises residues 218-289. Amyloid fibrils of HET-s(218-289) are necessary and sufficient for the induction and propagation of prion infectivity. We used fluorescence measurements, quenched hydrogen exchange NMR and solid state NMR to determine the sequence specific positions of secondary structure elements of the amyloid fibrils of HET-s(218-289). This information revealed four beta-strands constituted by two pseudo repeat sequences, each forming a beta-strand-turn-beta-strand motif. We showed that this conformation is the functional and infectious entity of the HET-s prion by using a structure-based mutagenesis approach. These results correlate for the first time distinct structural elements with prion infectivity.